Anticipating global warming effects: A comprehensive study of drought impact of both flax plants and fibres

Alessia Melelli, Sylvie Durand, Camille Alvarado, Antoine Kervoëlen, Loïc Foucat, Marie Grégoire, Olivier Arnould, Xavier Falourd, Franck Callebert, Pierre Ouagne, et al.

https://doi.org/10.1016/j.indcrop.2022.115011 Industrial Crops & Products 184 (2022) 115011

Anticipating global warming effects: a comprehensive study of drought impact of both flax plants and fibres

[a]Alessia Melelli, [b]Sylvie Durand, [b]Camille Alvarado, [a]Antoine Kervoëlen, [b,c]Loïc Foucat, [d]Marie Grégoire, [e]Olivier Arnould, [b,c]Xavier Falourd, [f]Franck Callebert, [d]Pierre Ouagne, [b]Audrey Geairon, [b]Sylviane Daniel, [g]Frédéric Jamme, [h]Caroline Mauve, [h]Bertrand Gakière, [a]Alain Bourmaud,*[b]Johnny Beaugrand

[a]Univ. Bretagne Sud, UMR CNRS 6027, IRDL, Lorient, France

[b]UR1268 Biopolymères Interactions Assemblages, INRAE, Nantes, France

[c]INRAE, BIBS facility, PROBE infrastructure, F-44316 Nantes, France

[d]Laboratoire Génie de Production, LGP, Université de Toulouse, INP-ENIT, Tarbes, France

[e]LMGC, Université de Montpellier, CNRS, Montpellier, France

[f]Groupe Depestele, 14540 Bourguébus, France

[g]Synchrotron SOLEIL, DISCO beamline, Gif-sur-Yvette, France

[h]Plateforme Métabolisme-Métabolome, Institute of Plant Sciences Paris-Saclay (IPS2), Université Paris-Saclay, National Committee of Scientific Research (CNRS), National Institute for Research for Agriculture, Food and Environment (INRAE), Université d'Evry, Université de Paris, 91190 Gif-sur-Yvette, France

*Corresponding author: johnny.beaugrand@inrae.fr

Abstract

Currently, the effects of global warming are one of the most important topics on the agendas of all governments and international economic and scientific organizations on the planet. Temperatures and rainfall will be especially subjected to increasing deregulation, and thus crop yields will be affected according to geographic location. Cellulosic materials, such as bast fibres, are considered one solution to decrease human environmental impact: they are a renewable resource, biodegradable and have a lower carbon emission than synthetic materials. However, their quality, yield and mechanical properties depend on environmental conditions during plant growth. In this paper, we explored the possible impact of seasonal drought linked to future climate change on flax plants and fibre quality. Two batches of the same textile flax plant cultivar were grown under two different field environmental conditions in the same year, one taken as a control under regular climatic conditions and the second one grown under drought stress. Carbon isotopic discrimination reveal an increase in water stress plant of the fibre $\delta^{13}C$, reflecting that plants are indeed suffering from drought stress from a physiological point of view. We characterized the mechanical properties, biochemistry and morphology parameters at both the stem and technical fibre scales. Our results showed that the plants of the two batches were morphologically different and that the drought-stressed plants were smaller, mainly in terms of the height of the stem (-28%) and diameter (-16%). Biochemical analyses highlighted a contrasting lignin content between the two batches. A difference in protein content was also measured, with an increased amount in stressed flax plants, with contrasting

distributions revealed by tyrosine and tryptophan monitored by synchrotron UV fluorescence. In addition, polysaccharide composition was also quantified with an increase in mannose and an important decrease in glucose in the drought-stressed technical fibres. Surprisingly, despite the difference in biochemistry composition and morphological parameters, the mechanical properties of elementary flax fibres extracted from the two batches were not significantly different. This suggests that drought can affect the yield and biochemistry of the extracted technical flax fibres but does not necessarily impact the longitudinal mechanical performance of single fibres.

Keywords: isotopic analysis; hydric stress; biochemical composition; mechanical properties, climate change

1. Introduction

In the last 20 years, the production of textile flax fibres and tows has increased considerably, and in 2019, the Food and Agriculture Organisation of the United Nations (FAOSTAT, www.fao.org) estimated the total world production to be up to 1,000 k tons, led by France with 85% of the world textile flax fibre production (Gomez-Campos et al., 2021; Manian et al., 2021). The renewed interest in flax and other plant fibres used in areas other than textile applications, such as composite design and engineering, is due in part to global warming and the low environmental impact of flax fibre production, especially compared to synthetic fibres (Le Duigou et al., 2011).

However, the production demand for plant fibres continues to grow with the goal of replacing synthetic fibres wherever possible and during the coming years, agriculture will have to increasingly contend with the effects of climate change. The reduced rainfall and the increment in temperatures implies the risk of abiotic stress such as drought, as well as various biotic stresses, for example, the emergence of new diseases and pests (European Environment Agency, 2019). Moreover, this same document also reports that the risks of heavy rainfall events and flooding, which contribute to crop damage, are increasing. Thus, to meet market demand, not only for flax but also for agricultural production more generally, farmers might be forced to use more irrigation or even phytochemical products to increase crop production, which may, at the same time, contribute to the drivers of climate change (**Figure 1**).

Focusing on France, textile flax crops are mainly located in Normandy and northern France (**Figure 2a**). The rapid increase in flax technical fibres and production during the last two years is reported in **Figure 2b**. It is worth noting that during 2001 and, particularly 2011, production recorded a violent decrease, and these years coincided with severe periods of drought (Audran and McLeod, 2011; Spinoni et al., 2015). Consequently, total world production was affected. Several models in the literature show the possible impact of climate change in European countries. Habets and Viennot reported a scenario with an increase in temperatures between 0.6 °C and 1.3 °C in 2021–2050 and a general decrease in rainfall in the entire country of approximately 6%, as illustrated in **Figure 2c** with a schematic readaptation of their maps (Habets and Viennot, 2015).

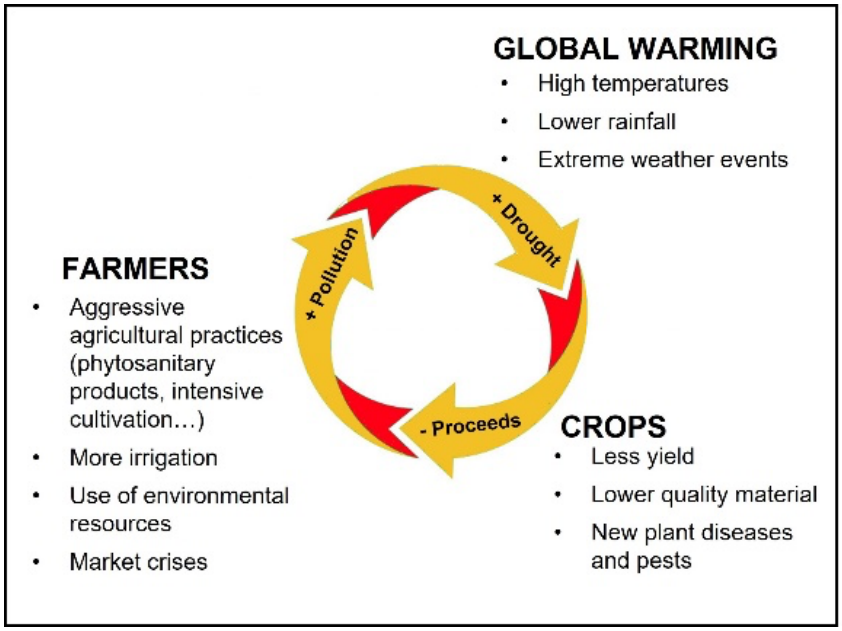

Figure 1 Synthetic representation of interactions between climate change, agricultural markets and crop management.

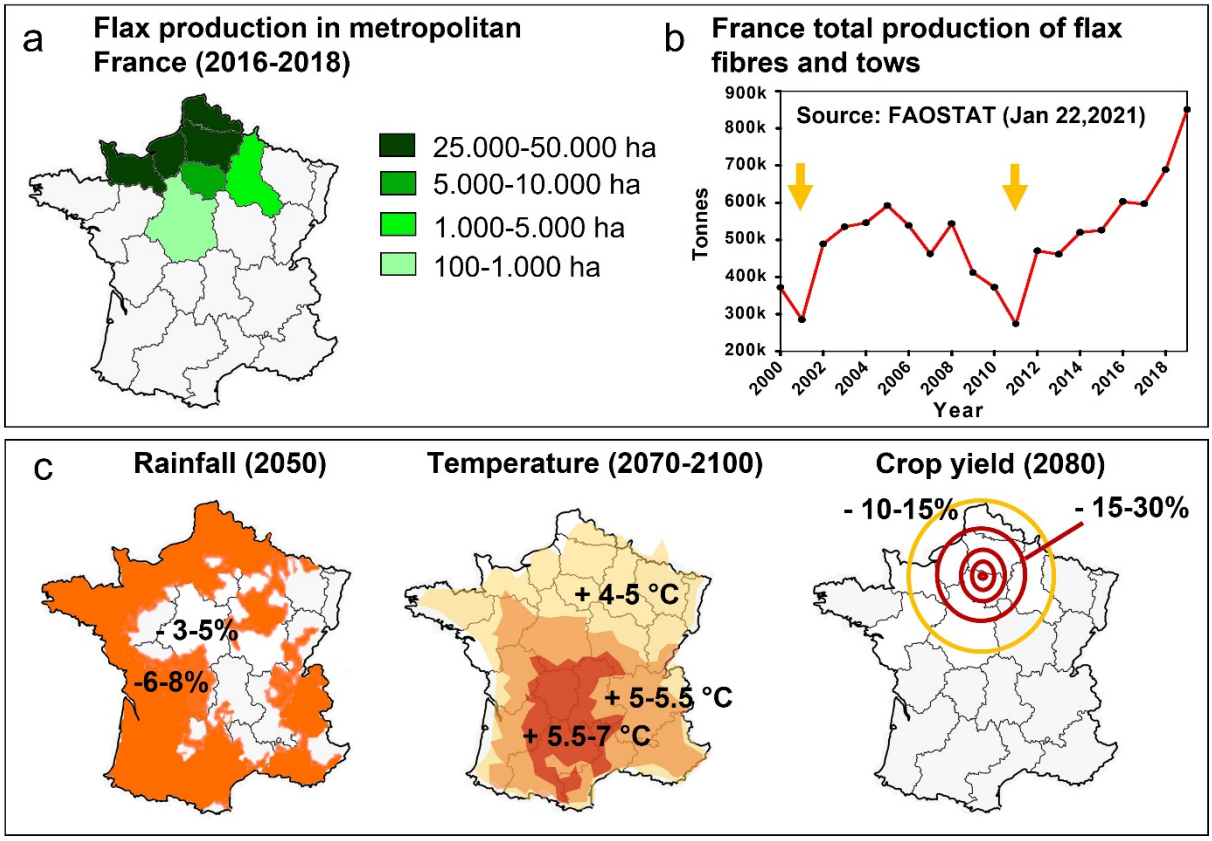

Figure 2 a) Map of flax production in France, adapted from FrD and IAR (Goulard et al., 2020), **b)** Production in France of tow and fibres between 2000–2019, data and graphic elaborated from FAOSTAT ("Crops and livestock products: flax fibre and tow," 2021). ; the yellow arrows indicate the drought that occurred in 2001 and 2011; **c)** Models of rainfall, temperature and crop yield readapted from (Habets and Viennot, 2015) and (Kelemen et al., 2009). Temperature and crop yield maps are simulations of changes compared to the years 1961-1990. Maps inspired from "PRUDENCE" and

"PESTEA" EU projects (Kelemen et al., 2009). Map: adapted from FrD and IAR (Goulard et al., 2020).

The European Commission has also published an official document in which several models are proposed to forecast the years 2070 to 2100 (Kelemen et al., 2009). In the worst-case scenario, if no actions are taken, northern France could be subjected to a temperature increase of approximately 4–5°C compared to the years 1961-1990. Moreover, in two different simulations, HadCM3/HIRHAM and ECHAM4/RCA3, compared to 1961-1990, northern France appears particularly impacted in terms of crop yield, with the highest loss of approximately 15%–30% due to drought and water deficiency (Kelemen et al., 2009). **Figure 2c** shows a schematic synthesis elaborated from the temperature and crop yield maps that can be found in the official document by Kelemen et al. (2009). All these data suggest that, in the future, flax fibre production could be particularly impacted since the cultivations are rather limited to a small area (northwestern France) that would be particularly subjected to the impact of climate change due to global warming. Thus, composite materials reinforced with plant fibres, especially flax, which appears to be a good alternative to other synthetic fibres, would no longer be sustainable in terms of CO_2 emissions, water irrigation and crop cultivation. Today, some agronomical practice and understanding of the crop physiology could help in limiting some effect of climate changes and their harmful effects on plants. For instance, natural biofertilizers as bacteria can confers a certain tolerance to drought stress to plant, as reported for soybean (Sheteiwy et al., 2021) that could counterbalance in part the harmful effects of drought. In addition, for some species, like maize inbred lines that are chilling tolerant or not, it was shown that modulators of biological processes sensitive to chilling are positively correlated with root length and shoot fresh weight of seedling (Gao et al., 2020).

The effect of water deficit on plants has already been studied for several fibre plant species, such as ramie, flax or hemp. At the crop level, the consequences of particularly hot and dry years were observed with a decrease in the yield and quality of the product, as in the case of linseed oil (Jaime et al., 2018). For other species, such as hemp, drought leads to the formation of morphologically thinner and heterogeneous cell walls, probably caused by a delay in their maturity and thickening process (Abot et al., 2013).

In the case of flax, it has been observed that moderate soil drought affects plants that produce a low number of ramifications, with a reduction in the number of leaves and a decrease in stem length (Chemikosova et al., 2006; Kariuki et al., 2016; Milthorpe, 1945) and roots (Mahfouze et al., 2017). In the case of severe drought, cessation of metabolic processes was observed (Chemikosova et al., 2006). At the cell scale, flax fibres extracted from drought-stressed plants were found to be shorter than those extracted from plants grown in nonstressed conditions. Moreover, a modification of the polysaccharides was observed with a decrease in the galactose/rhamnose ratio (monosaccharides), a change in the number and length of rhamnogalacturonan-I chains and, consequently, an increase in the disorder of the cellulose microfibril network (Chemikosova et al., 2006).

However, the origin of the domesticated flax plant is ancient; it was cultivated for millennia in Mesopotamia, Syria and Egypt (Bedigian and Harlan, 1986; Michel and Nosch, 2010), and these regions are particularly dry and hot, much more than the

climate we find in northern France. Since flax needs approximately 400 mm of rainfall in 120 days of growth (ARVALIS Institute du végétal, 2015), depending on the water-holding capacity of the soil, and since drought or temperatures higher than 35 °C during and after flowering reduce the yield and quality of both fibres and linseed oil, certain practices were used in ancient times to compensate for the lack of water. For instance, in the ancient Near East, flax was sown in irrigated soils (Bedigian and Harlan, 1986). In the case of ancient Mesopotamia, the culture of flax was limited to very small lots rich in water and clays (Bedigian and Harlan, 1986), and in ancient Egypt, flax cultivation started in November following the Nile floods (Vogeslang-Eastwood, 2000).

In this context, the present work aims to investigate the consequences of drought on flax plants and the impact on the mechanical properties of elementary flax fibres for industrial batches of the same variety sown on the same date in two different selected areas of Normandy (France), one subjected to drought conditions and the other well irrigated when necessary and taken as a control, to evaluate the response to drought stress at both the plant and fibre levels. Originally, the scientific approach proposes to couple mechanical, ultrastructural and biochemical investigations to deeply explore and discuss the effect of drought on flax fibres.

2. Materials

Two batches of the Damara flax industrial variety were sown at the end of March 2019 by the Depestele Group, a French company specializing in flax culture and processing, in two different growing areas located in Ernes (control; 90 cm silt on limestone irrigated sowed in March 25th) and Fourches (at risk of drought, 25-30 cm clay-limestone soil on limestone, not irrigated, sowed in March 22nd), in Normandy (France). The two areas are approximately 20 km away from each other and sowing was done with the same seed rate of 1900 seeds/ meter square. The agronomic practices (fertilizers applied, plant protection measures) were standards. During the whole fibre growth period, rainfall was constantly recorded until harvesting (**Figure 3a**) together with temperature and relative humidity (**Figure 3b**). Damara is a textile flax variety registered in the official catalogue of varieties since 2011. It has a marked sensitivity to lodging but is known to be tolerant to water stress. In 2020, the harvest in France had an average yield of 25.4% in long fibre and 43.2% in total fibre.

It is important to note that the problem of defining drought from a meteorological or agricultural point of view was already discussed in (Wilhite and Glantz, 1985), with the conclusion that a lack of precipitation does not necessarily coincide with agricultural drought, expressed as the water demand of the plant. In the present study, it was defined drought as the batch that received less than 100 mm of cumulated rainfall and without irrigation, contrary to the 400 mm generally required. In contrast, the control batch was grown with nearly 250 mm of cumulative rainfall and irrigated when necessary, in order to reach the water demand of flax.

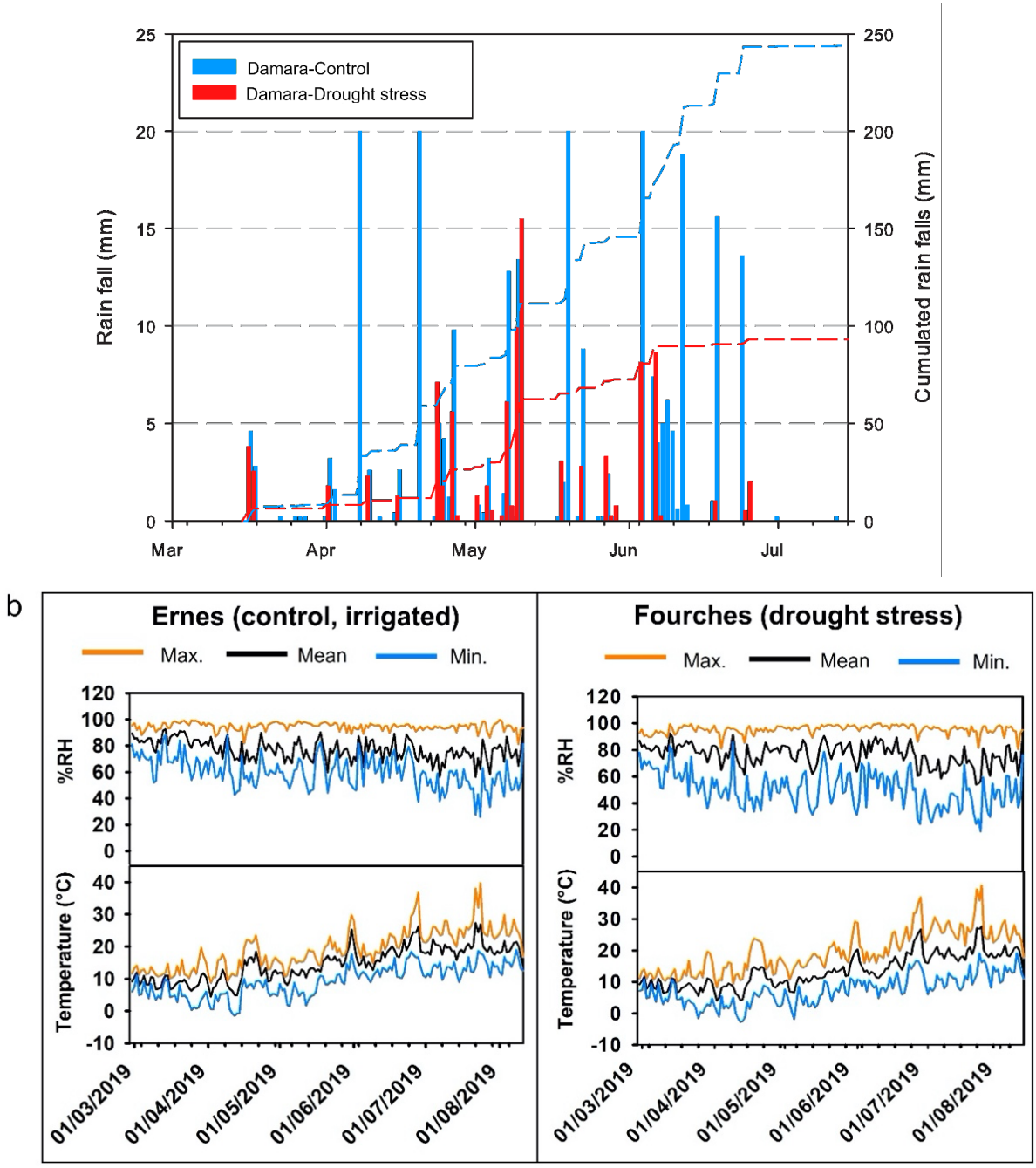

Figure 3 a) Daily (histograms) and cumulative (dotted lines) rainfall for the two cultivation areas; b) Temperatures and relative humidity recorded during the plant growth of the two crops in selected cultivation areas.

A group of approximately 100 plants were sampled from both cultivations before harvesting and at the beginning of July after approximately 103 days of growth. Fifteen stems were randomly selected to calculate height and diameter to obtain a representative sample, and the other 3 stems were randomly selected and prepared for observations at the DISCO (Dichroism, Imaging and mass Spectrometry for Chemical and biOlogical systems) beamline. The rest of the crop was harvested, and dew was retted *in situ* by the Depestele Group (beginning of retting on July 11th in Fourches and on July 16th in Ernes) until the middle of August (12-19 August). Fibres were successively extracted using pilot (lab-scale) scutching/combing equipment

equipped with a small line with three modules for breaking, scutching and combing (more precisely described in (Réquilé et al., 2021). Stems passed three times through the breaking module, once in the scutching module and two times in the hackling module.

3. Methods

3.1. DISCO Beamline Synchrotron Facility

3.1.1. Sample preparation

A segment of 6 cm was cut at the middle height of the plant of the three fresh stems selected from each of the two batches (**Figure A.1**). Three small segments of 0.5 cm were successively obtained from the small portion of each individual stem, avoiding the first millimetres in direct contact with air, and then fixed at 4 °C for 24 h in a FAA (formalin acetic acid alcohol) fixative mixture of 10:5:85 v/v composed of formaldehyde (37%), glacial acetic acid (60%) and ethanol (95%). Samples were then transferred to an automatic tissue processor (Automatic Tissue Tek VIP 3000, Sakura, MI, USA) for ethanol dehydration and successive inclusion in paraffin. Sections were successively cut with a thickness of 10 µm and placed between two quartz coverslips (Circular-Quartz, Ref. R525000, Esco Optics, USA).

The sections were treated with a HistoChoice Clearing Agent (H2779, Sigma) solution to remove paraffin. To detect lignin, stem samples were stained using Wiesner (phloroglucinol-HCl) reagent as described in Bouvier d'Yvoire *et al.* (Bouvier d'Yvoire et al., 2013). Cross-sections were immediately observed using a macroscope (AZ100 M, NIKON, Japan) under bright-field conditions.

3.1.2. Set up

Two different microscopes of Synchrotron SOLEIL (Source Optimisée de Lumière d'Energie Intermédiaire du LURE) (Gif-sur-Yvette, France), DISCO beamline, were used to obtain different information: a full-field microscope, called TELEMOS, that allows multispectral fluorescence imaging analysis and an inverted microscope adapted to perform scanning fluorescence microspectroscopy, called POLYPHEME.

TELEMOS parameters

The excitation wavelength used was in the deep UV range (275 nm), extracted from the white beam and monochromatised, thanks to a Czerny-Turner monochromator (iHR320, Jobin-Yvon, France) before reaching the end-stations, as described in (Jamme et al., 2010, 2013; Séverin-Fabiani, 2016). The entire beamline is fully described in (Giuliani et al., 2009). TELEMOS is a full field Axio Observer Z1 inverted microscope (Carl Zeiss GmbH, Germany) modified with quartz optic and equipped with a dichroic mirror at 300 nm (Omega Optical Inc., Brattleboro, USA), which allows the reflection of the excitation wavelength at 275 nm and cutting all the wavelengths above 300 nm, a back-illuminated CCD 16-bit camera (Pixis BUV, Princeton Instrument, USA) and a motorised sample plate (MS-2000 XY, Applied Scientific Instrument, USA), which allows movements in the X- and Y-axes. The Z-axis is directly controlled by the microscope. More details about the equipment can be found in (Jamme et al., 2010; Séverin-Fabiani, 2016; Devaux, 2018; Vidot et al., 2019). Specific objectives for UV

transmission, 10x (N.A. 0.2) and 40x (N.A. 0.6) Ultrafluar (Zeiss) with chromatic correction were used to investigate the samples.

Three different passband filters at 327–353, 420–460, and 480–550 nm (Semrock, Rochester, USA) were used in this work to obtain information about: 1) protein, by probing their tyrosine and tryptophan amino acids, 2) small phenolic compounds called hydroxycinnamates (ferulic, *p*-coumaric and sinapic acids), and 3) lignin, as a polymer composed of 3 phenyl propanoid units (G, H and S) respectively (Devaux, 2018). Time and offset for image acquisition were adjusted according to the objective used (**Table 1**). Further details are given in the Supplementary Appendix.

Table 1 Deep UV acquisition parameters with TELEMOS microscope and possible attributions.

Filter	Acquisition time (s)	Objective	Attribution	Channel
327-353 nm	8 20	x10 x40	proteins (Tryptophan and Tyrosine)	Red
420-460 nm	8 8	x10 x40	Phenolic compounds (hydroxycinnamic acids…)	Green
480-550 nm	8 8	x10 x40	Lignin (phenyl propanoid units)	Blue

The choice of these three filters was made after previous investigations on flax stems (Beaugrand et al., 2022). A t-test using Sigmaplot was calculated to establish the confidence of the calculated values obtained as shown in **Figure A.2**. The images presented in this work are composite images resulting from the sum of the three filters assigned to the RGB channels.

POLYPHEME parameters

POLYPHEME is an Olympus IX71 inverted microscope modified with a quartz optic suitable for deep UV (DUV) spectroscopy equipped with a triple monochromator (T64000, Jobin-Yvon) in subtractive mode to suppress Rayleigh scattering and another 280 nm beam splitter. To collect spectra, an iDus CCD detector (Andor) was used (Peltier cooling to -70°C). The detector is a 1024x256 pixel with 26x26 µm pixels (Jamme et al., 2010). The objective used was a 40x Ultrafluar (Zeiss) objective with N.A. 0.6 and a laser spot diameter of approximately 4 µm.

Before collecting the spectra, a calibration using the Nd-YAG crystal was performed. Due to limited time, only two cross-sections, one drought and one control, were examined under POLYPHEME. After acquisition, the spectra were processed using LabSpec 6 (Horiba Scientific) software and a program file written in MATLAB, Polypheme v2.0. Each spectrum was cut in the range of 294–529 nm. A correction of dead pixels at 323.7–323.2 nm was performed followed by spike correction. No smoothing operation was performed. Subsequently, MATLAB was used to calculate the principal component analysis after concatenating the two images acquired from the two different samples, and spectra were normalised using a unit vector ($\frac{x}{\sqrt{S^2}}$). The 'modelling' tool of LabSpec 5 (Horiba Scientific) software was successively used to

create a normalised model where the score combination reached 100% by selecting three components identified as the three main signals of the spectra at approximately 335, 415 and 500–530 nm, obtaining separate cartographies of protein, phenolics and lignin. An example of the corrected spectra and a table with the proposed fluorescence emission assignments are illustrated in **Figure A.3** and **Table 2**.

Table 2 Possible attribution of fluorescence emission collected with POLYPHEME microscope.

Emission	Attribution	Reference
≈ 306 nm	Tyrosine	(Tedetti et al., 2012; Jamme et al., 2013)
≈ 335 nm	Tryptophan	(Tedetti et al., 2012; Jamme et al., 2013)
≈ 415 nm	Ferulic Acid	(Jamme et al., 2013)
≈ 435 nm	Caffeic Acid	(Vidot et al., 2019)
≈ 480 nm	Lignin	(Jamme et al., 2013)
≈ 500-530 nm	Lignin	Disco beam line team personal communication

3.2. Single fibres tensile tests

Between 58 and 60 flax fibres were extracted from each batch and glued with universal glue on paper support according to ASTM C1557 (*ASTM C1557-20*, 2020), with a gauge length of 10 mm. The average diameter of each fibre (approximating the fibre to be perfectly cylindrical) was manually calculated considering five points of measurement under an optical microscope, as described in (Lefeuvre et al., 2014). The sample elementary fibres were tensile tested by a universal MTS Synergy testing machine equipped with a load cell of 2 N under a controlled atmosphere (T= 23±2°C; %RH = 50±4%) thanks to a Liebert Hiross indoor room cooling unit. The crosshead displacement rate was set at 1 mm/min until the fibre broke. The determination of the tensile properties, i.e., Young's modulus (E, GPa), strength at rupture (σ, MPa) and strain at rupture (ε_r, %) were determined by taking into account the compliance of the loading frame.

3.3. Mechanical investigation of flax cell walls by AFM and Nanoindentation

3.3.1. AFM PF-QNM analysis

After that the stems of the two batches were scutched with the scutching line machine, several technical fibres extracted with a scutching line machine after the stem dew retting process were embedded using a low viscosity epoxy resin kit from Agar Scientific (UK) using a flat mould. The full procedure concerning the samples preparation lightly dried in an oven, the final polymerization of the blocks and the surface preparation by ultramicrotome is described in (Melelli et al., 2021).

A Multimode 8 AFM microscope AFM instrument (Bruker, Billerica, MA, USA) was used in Peak Force Quantitative Nanomechanical Property Mapping (PF-QNM) mode, and the instrument was calibrated following the method in (Melelli et al., 2021). The peak force amplitude was set at 50 nm, the maximum load was 200 nN, and a tip radius

between 25 and 99 nm was obtained by calibration with a spring constant between 111 and 194 N/m following the same procedure as in (Melelli et al., 2020, 2021). The gain was set to automatic. At least 8 images for each batch were acquired and used to calculate the mean. All the acquisitions were made at controlled temperature (T = 23±2°C) and relative humidity (%RH = 50±4%).

3.3.2. Nanoindentation

Nanoindentation analysis was performed on the same blocks prepared for AFM, and 24 tests for the control and 38 tests for drought-stressed flax fibres were performed. Nanoindentation analysis was carried out by a Nanoindenteur XP (MTS Nano Instruments, Oak Bridge, Tennessee, USA) used at controlled atmosphere (T = 23±2°C; %RH = 50±4%). The instrument was equipped with a three-sided pyramid indenter (Berkovich-Berko XPT-12761–0) and a 40x objective. The strain rate was set at 0.05 s^{-1} (i.e., 1 μN/s) during loading to reach a depth limit of 120 nm. The load was held at the maximum value for 60 s, and then withdrawal was performed with the same loading rate up to 10% of the maximum load. At least 20 locations in each sample for each batch were tested.

3.4. Biochemistry

3.4.1. Sample preparation for biochemical analysis

Ten flax stems were cut into 3 segment equivalents in length, and the middle part was retained for further biochemical analysis. The middle segment was manually peeled, and both the flax bundles and the shive part were collected and pooled by sample nature. The content of the monosaccharides was then quantified by operating a homogenization step by cryogrinding (SPEX 6700 freezer Mill) approximately 1 g of the sample.

3.4.2. Monosaccharides

The protocol was slightly modified from Barteau *et al.* (2021) in the presence of inositol as an internal standard. Neutral monosaccharides were analysed as their alditol acetate derivatives (Blakeney et al., 1983) by gas chromatography-flame ionization detection (GC-FID) (Perkin Elmer, Clarus 580, Shelton, CT, USA). For calibration, standards of carbohydrate solutions were used. Analyses were performed in three independent assays. The total monosaccharide content is the sum of each monosaccharide amount and is expressed as the percentage of the dry matter mass.

3.4.3. Lignin

The lignin content was quantified in homogenised powdered particles of samples. Lignin was assessed by spectrophotometry following the acetyl bromide method (Hatfield and Fukushima, 2005) on samples of approximately 20 mg in mass weight per assay. The chemicals were laboratory grade from Sigma Aldrich, and the analyses were performed with four independent assays, with the lignin content expressed as a percentage of the dry matter mass.

3.4.4. Proteins

The total C and N contents of the samples were determined on cryogrinded powders via the Dumas method using an elemental analyser (VarioMicro, ELEMENTAR). Protein contents were determined from N contents multiplied by a 5.7 coefficient usually applied for non-reserve proteins. Experiments were run in triplicate with a calculated experimental error of less than 5%.

3.4.5. Hydroxycinnamic acids

Ester-linked phenolics from bast fibre and shives were analysed after mild alkaline hydrolysis according to the protocol in (Ho-Yue-Kuang et al., 2016). For this purpose, 1 mL of 1 N NaOH was added to the ground samples (approx. 10 mg per assay) in centrifuged tubes and incubated for 4 h at 40 °C in a ventilated oven. Tubes were then centrifuged to discard the remaining particles, and the reaction media was acidified with 200 µL of 6 M HCl. After centrifugation (12,000 rpm, 10 min), supernatants were deposited onto a solid-phase extraction cartridge (Waters Sep-Pak Plus Short tC18 cartridges) that were preconditioned before use. Washes and elution were conducted with 1 mL solutions. The samples were then concentrated six times using an air evaporator concentrator, filtered (0.45 µm) and analysed by high-performance liquid chromatography (HPLC) combined with UV diode array detection (HPLC-DAD). The samples (2 µL) were injected onto an RP18 column (Macherey Nagel 2 × 50 mm 2.7 µm particle size, Nucleoshell RP18plus) with a flow rate of 0.3 mL.min^{-1}. The eluents were 0.1% formic acid in water (A) and 0.1% formic acid in acetonitrile (B), with a gradient of B until 60%. Peak assignment from chromatograms was performed at 320 nm according to their retention time by comparison with well-characterised samples of maize bran and UV absorption spectra (Waldron et al., 1996). A calibration curve with ferulic acid at different concentrations was used for quantification.

The supramolecular organisation of macromolecules was investigated by two complementary techniques: i) ^{13}C NMR cross polarisation-magic angle spinning (CPMAS), and ii) variable contact time cross-polarisation magic angle spinning ^{13}C VCT-CPMAS.

3.4.6. ^{1}H and ^{13}C NMR CPMAS

Solid-state NMR (ssNMR) spectra were registered on a Bruker Advance III 400 spectrometer on rehydrated AIM to approximately 30% (w/w) with ultrapure H_2O. Spectra were recorded at a proton frequency of 400.13 MHz and a carbon frequency of 100.62 MHz. A double resonance ^{1}H/X CPMAS 4 mm probe was used. The magic-angle-spinning (MAS) rate was fixed at 12 kHz, and each acquisition was recorded at room temperature (293 K). CPMAS experiments were realised using a 90° proton pulse of 3.3 µs, a contact time of 1.5 ms and a 10 s recycling time for an acquisition of 34 ms during which dipolar decoupling (SPINAL64) of 37.8 kHz was applied. Typically, 2048 scans were accumulated per spectrum. Chemical shifts were calibrated with external glycine, assigning the carbonyl at 176.03 ppm.

The approach developed by Larsson et al. (1997) was used to evaluate the cellulose crystallinity from the deconvoluted C_4 peaks in the region 77–92 ppm. In the crystalline part of the region (Cr), the Larsson *et al.* method was performed thanks to the use of three Lorentzian peaks corresponding to cellulose Cr(I_α) (89.1 ppm), cellulose Cr(I_α+I_β)

(88.2 ppm) and cellulose Cr(I_β) (87.2 ppm) (Larsson et al., 1997). An additional Gaussian peak representing the paracrystalline (PCr) contribution (88.1 ppm) is also used.

Three peaks were used in the amorphous C_4 region: two Gaussian peaks corresponding to accessible surface cellulose C_4 (AS; 82.7 and 83.7 ppm) and another peak corresponding to inaccessible surface C_4 (IAS; 83.4 ppm). The proportion of crystalline cellulose in the different samples was determined by dividing the area of the three peaks of the crystalline region by those of the six peaks for the cellulose C_4 region. The lateral dimensions of the fibrils (LFD) and the lateral dimensions of the fibril aggregates (LFAD) were then estimated assuming a square cross-section of cellulose microfibrils. These estimates assumed that all amorphous cellulose was on the fibril surface. The cellulosic chain width was taken as 0.57 nm (Newman, 1999).

The chemical shift, half-width and area of peaks were determined using a least-squares fitting method using Peakfit® software (Systat Software Inc., USA).

3.4.7. ^{13}C VCT-CPMAS

By varying the contact time τ of cross-polarisation (20 points between 10 µs and 9000 µs, with 512 accumulations per experiment), the dynamics of cross-polarisation were investigated. It is often presumed that magnetisation in ^{13}C rises exponentially with time constant T_{CH} and then decays with time constant $T_{1\rho}^H$ so that the two time constants can be extracted by fitting a dual exponential function (Kolodziejski and Klinowski, 2002). Nevertheless, it has become clear that the rising part of the curve is too complex to be described by a single exponential but rather comprises a rapid and a slower phase. Depolarisation of ^{13}C in the rotating frame is described by single-phase kinetics. The cross-polarisation kinetics were fitted with the following formula (**Equ. 1**) (Kolodziejski and Klinowski, 2002), and minimization was performed with the Excel solver:

$$I(\tau) = I_0 e^{-\tau/T_{1\rho}^H} * \left\{1 - \lambda e^{-\tau/T_{HH}} - (1-\lambda) e^{-3\tau/2T_{HH}} e^{-\tau^2/2T_{CH}^2}\right\}, \quad (1)$$

where $I(\tau)$ is the area of the carbon peak according to the contact time τ,
I_0 is the maximum carbon signal intensity (associated with the optimal contact time),
λ is a parameter that depends on the number of protons (n) carried by carbons (λ=1/(n+1)), T_{CH} is the mean dipolar coupling between carbon and proton covalently link, T_{HH} is the spin diffusion between the two proton reservoirs, and $T_{1\rho}^H$ is the rotating-frame spin–lattice relaxation time.

3.5 Carbon Isotopic analyses

One milligram of lyophilized frozen material was all placed in tin capsules and burned in an elemental analyser (Pyrocube Elementar, Villeurbanne, France). Separation of resulting N_2 and CO_2 gas on gas-selective columns with Thermal Conductivity Detector (TCD). These Gas go on isotope-ratio mass spectrometer (ISOPRIME Elementar, Villeurbanne, France) and Isotope composition (13C/12C) can be measured. These values were expressed in delta (δ13C) notation in permil, that is, as deviation of the

carbon isotope ratio from the international standard Vienna Pee Dee Belemnite: δ13C=(RsampleRV-PDB)/RV-PDB. Some International Atomic Energy Agency standards USGS-40 (glutamic acid, δ13C = -26.39‰), IAEA-601 (benzoic Acid, δ13C = -28.81‰) and IAEA-CH-6 (Sucrose, δ13C = -10.449‰) were measured every six samples to assess measurement accuracy and correct for any drift of the mass spectrometer. Experiments were done in triplicate.

4. Results

4.1. Impact of drought on overall stem architecture

The first observations were performed by collecting data on the height and diameter of 15 stems sampled at plant maturity. Despite the same seeding rate, the difference in height between the stems selected from the two batches was significant (t-test with $p \leq 0.001$) and was approximately 28%, with average length values of 81.8 ± 4.3 cm and 59.0 ± 6.5 cm for normal and droughted stems, respectively. In contrast, the difference in diameter, measured every 5 cm until the first branches, was less pronounced but still significant (**Figure 4**), especially in the middle and bottom of the stems. In the present study, control stems presented a height in line with the height of the Damara variety measured for 2019 in other flax lots (ARVALIS Institut du végétal, 2019).

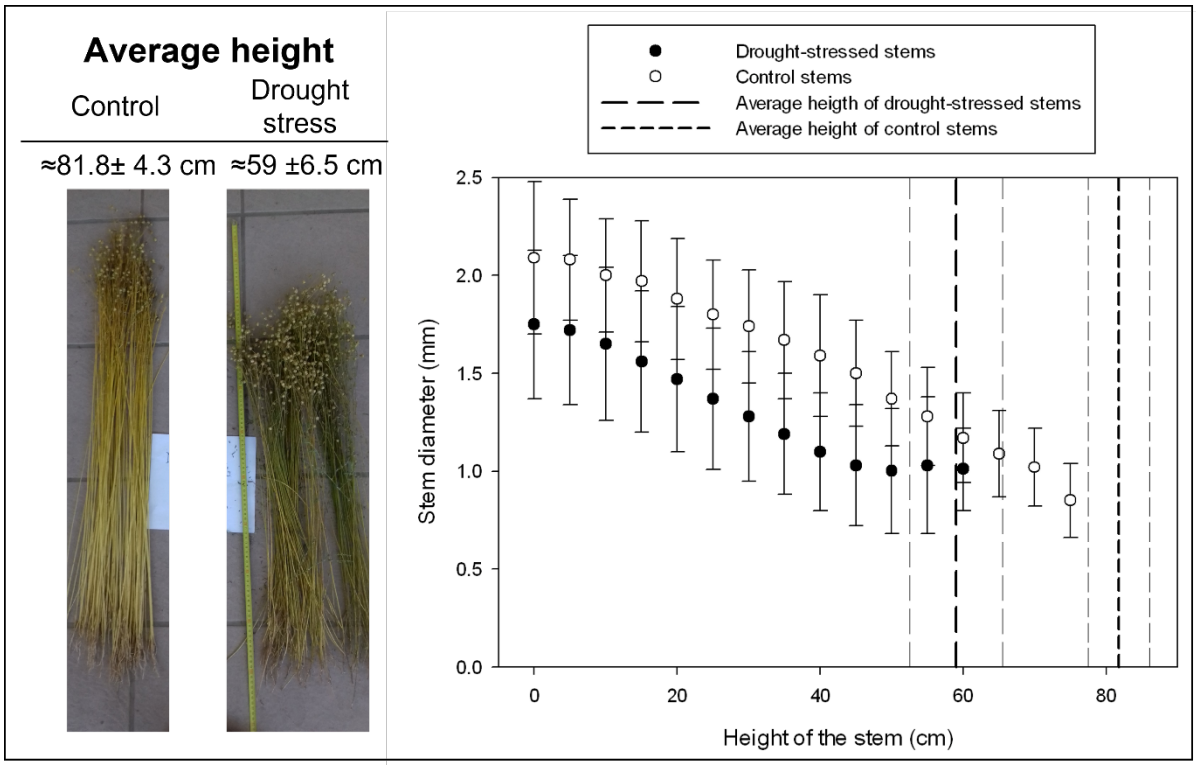

Figure 4. The height and diameter of 15 stems from the two batches with the relative standard deviations.

An important criterion to evaluate drought stress in flax plants is the yield after fibre extraction. In this case, the plants grown under drought conditions had a yield of 4.49 t/ha and a scutching yield of 13.8% against 7.19 t/ha and scutching yield of 17.2% of the control one; in general, the yield in terms of tonnes for the Damara variety is 8.54

t/ha, and the scutching yield should be approximately 20–28% under normal conditions (ARVALIS Institut du végétal, 2019).

In addition, to the significant lower yield of fibre in the drought flax plant, carbon isotopic discrimination was conducted to check that the flax plant suffered drought stress from a physiological point of view. The natural ^{13}C abundance ($\delta^{13}C$) has been widely used in agronomy to monitor strategies to balance carbon acquisition and water loss crop water use efficiency (WUE), indicating how plants respond to change in abiotic environmental factors such as drought stress (Farquhar et al., 1982 ; Cernusak et al., 2013). Control plant fibre bundles have an average $\delta^{13}C$ of -29.316 ± 0.05 when water deficient flax fibre have an -26.343 value. The $\delta^{13}C$ values measured in fibers of flax plants were significantly increased under drought conditions, revealing a long-term effect of drought on physiological parameter and indicating that plant cultivated under low-water diet effectively suffered from drought stress.

4.2. Impact of drought on biochemical composition of the stem

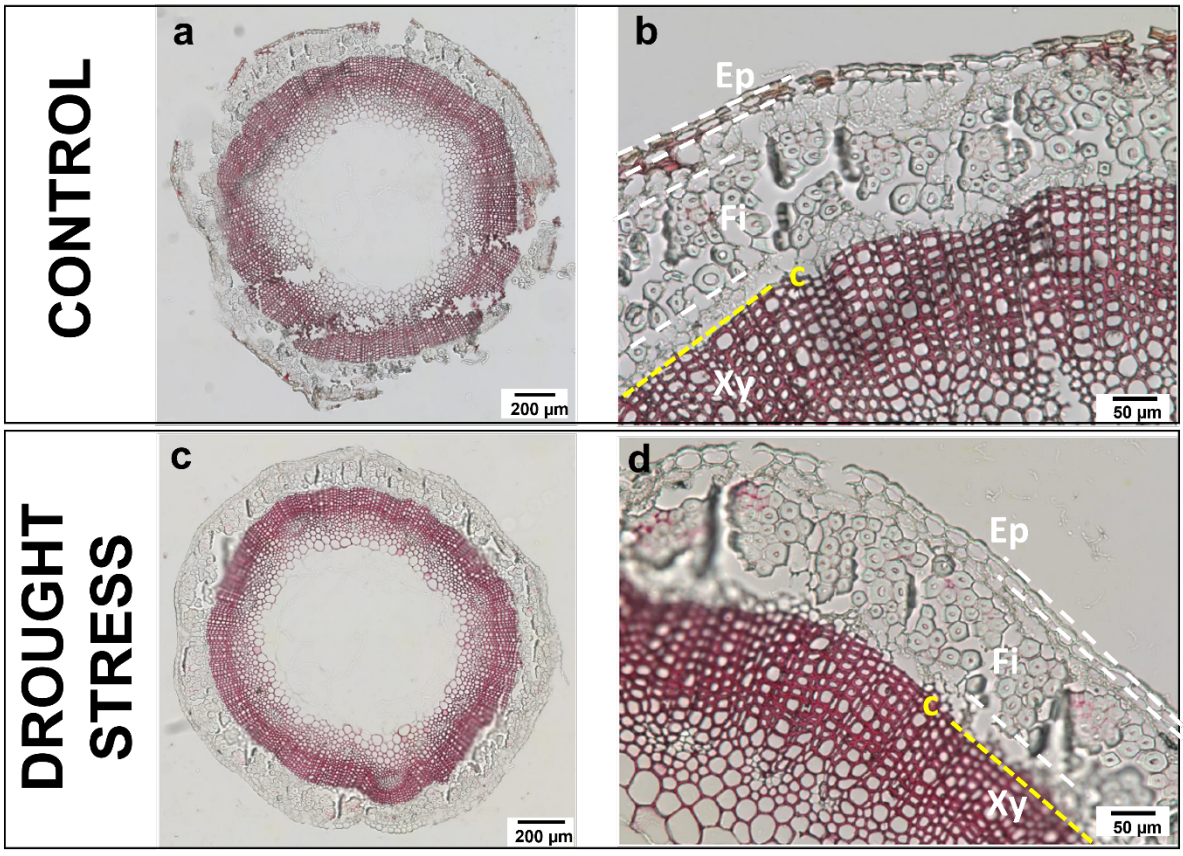

Figure 5. Overview of control and drought-stressed cross sections. Lignin is highlighted by phloroglucinol staining, and xylem is particularly rich in lignin. Three main tissues of interest are labelled here: Ep=epidermis, Fi= fibres, and Xy= xylem in white. The cambium (c) is highlighted in yellow. The cortical parenchyma between epidermis and fibres and the phloem between the fibres and the cambium are not considered in this case because they do not show any strong staining and their cells are too small to be evaluated. Objective 5x **(a-c)** and using 5x digital zoom **(b-d).**

Wiesner staining revealed coniferaldehyde end groups in lignin by red–purple colouration. An overview of a cross section of a control and drought stem does not show huge differences contrasted between the two batches (**Figure 5**) but highlight the xylem rich area on both control and drought stressed stems. Higher fluorescence emission in DUV fluorescence collected at 480–550 nm suggests more lignin in the drought-stressed stems (**Figures 6.a-f**), but it is contradicted by direct lignin quantification with the acetyl bromide method. No significant difference in lignin content appeared in the bast fibre region under naked eye observation (**Figure 5**).

Using synchrotron DUV, fluorescence imaging showed similar results obtained from images acquired under 40x (**Figure 6.e**) and 10x (**Figure 6.f**) objectives with TELEMOS microscope. The mean values from the control and drought-stressed plants were calculated using the three sections from each of the three stems.

Despite the important standard deviation, the fluorescence intensity collected between 480–550 nm, attributed to lignin, appeared higher in the epidermis of the stressed stems, while the cortical parenchyma did not show any particular changes, except that a higher variability was observed in the control stems than in the stressed stems.

The bast fibres were particularly interesting because in the drought-stressed stems, it was observed a higher fluorescence intensity at 480–550 nm, attributed mostly to lignin (**Figure 6.f**). Additionally, the fluorescence intensity due to tyrosine and tryptophan (327–353 nm) appeared higher in the drought-stressed fibres, but the p value calculated with the t-test indicated a nonsignificant difference, and for this reason, complementary direct biochemical analyses were performed. The phloem region from the control stems, as in cortical parenchyma, was demonstrated to have greater variability than that in the drought-stressed stems, especially regarding protein and phenolic compounds. In the xylem of the drought-stressed stems, a higher fluorescence intensity due to lignin and protein was noticed when calculated under the 40x objective. This trend was also recorded for the phenolic compounds.

The results obtained under DUV imaging were confirmed using POLYPHEME, recording a map of spectra of two cross-sections, one for each batch, chosen from the dataset. **Figure 7** shows averaged spectra, normalised using the integrals of the three main signals 300–340 nm (attributed to protein), 415 nm (attributed to ferulic acid) and 500–530 nm (attributed to lignin) and decomposed in three different mappings.

Signals attributed to protein (red map) seemed less well distributed in the drought stem cross-section. In the cortical parenchyma of the control stem, a high concentration of protein was observed, while in the drought-stressed stem, the distribution was inhomogeneous, and the fluorescence was apparently less intense. Only some of the drought-stressed fibres gave protein autofluorescence, while in the control stem, the fluorescence was extended to all the fibres.

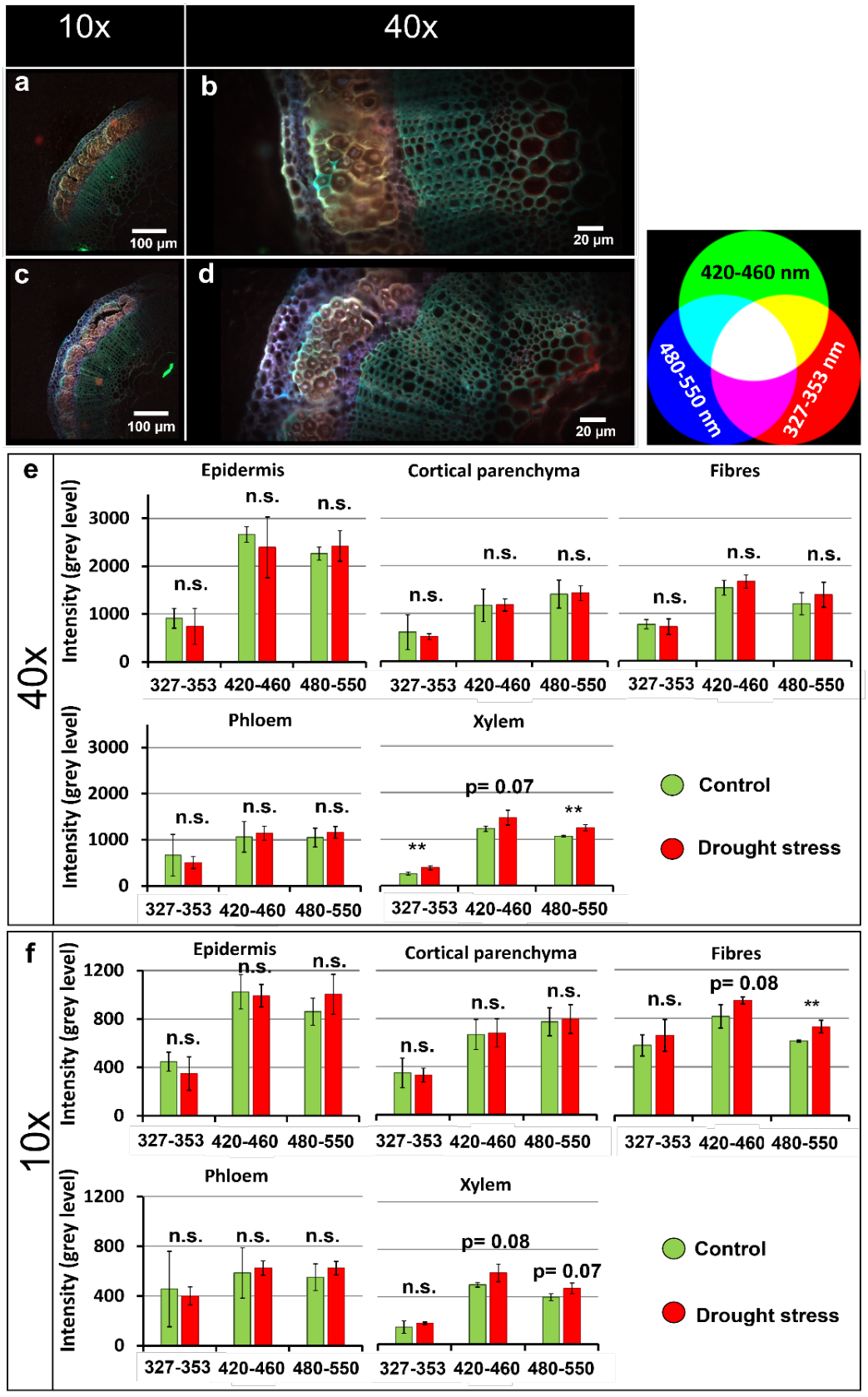

n.s.= p>0.05, * = p≤0.05, **= p≤0.01

Figure 6. TELEMOS images under 10x and 40x objectives with the three channels merged to create a single image in RGB of a-b) control stems and c-d) stressed stems. e-f) Graphs of the mean and standard deviation of the fluorescence intensity values calculated in each tissue considered.

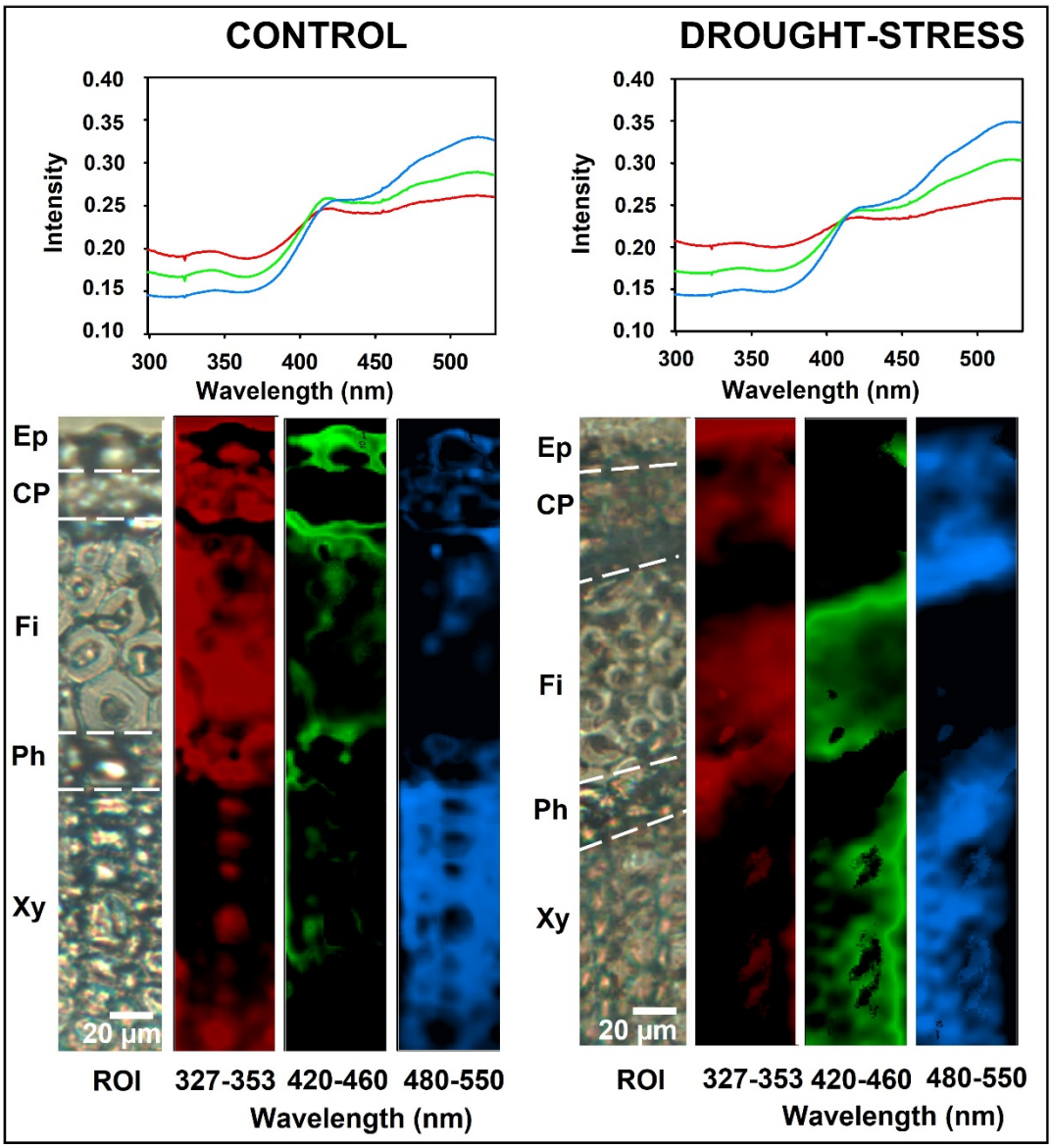

Figure 7. Two cross sections of the stems were investigated under fluorescence microspectroscopy (POLYPHEME). The spectra were averaged and normalised and three mappings were extracted to highlight signals attributed to protein (red), phenolic compound (green) and lignin (blue) distributions. Ep=epidermis, CP=cortical parenchyma, Fi=fibres, Ph=phloem, and Xy=xylem.

The distribution of fluorescence attributed to phenolic compounds (green map) and lignin (blue map) is more interesting. In the control stem, the epidermis was rich in phenolic compounds, while no fluorescence was recorded in the stressed stem. On the other hand, technical fibres and xylem of the drought-stressed stem appeared much more enriched in phenolic compounds than those of the control stem. Fluorescence attributed to lignin content did not seem to visibly change in the xylem of the two batches, but lignin was observed to be less localised and better distributed in the cortical parenchyma and epidermis cells of the drought-stressed stem.

4.3. Impact of drought on fibres composition and structure

Biochemical analysis of fibres extracted with GC-FID quantification showed a decrease of approximately 10% in total monosaccharide, approximately 15% of uronic acid and approximately 13% in glucose expressed in dry matter material for drought-stressed fibres (**Figure 8** and **Table 3).** Lefeuvre *et al.* (2018) attributed arabinose, rhamnose and galactose to RG-I and xylose, mannose and glucose to "hemicellulose". In contrast to Lefeuvre *et al.*, Akin *et al.* attributed glucose to cellulose content and designed the rest as noncellulosic polysaccharides, abbreviated as NCP (Akin et al., 1996). These last authors calculated a ratio between glucose and the sum of xylose, rhamnose, galactose, mannose and arabinose (NCP), to which a small amount of fucose was added. In the present study, glucose was assumed to be indicative of cellulose.

In drought-stressed flax fibres, the mannose content was increased by 28% and the ratio of Glucose/NCP in stressed flax bundles was lower, 4.9 in stressed fibres compared to 6.5 in control fibres as reported in **Table 3**. This is probably due to both a higher quantity of NCP and a slight decrease in cellulose. These observations are consistent with those of Lefeuvre *et al.*, who reported an increase in hemicellulose polysaccharides (Lefeuvre et al., 2018).

Regarding lignin, a significant increase of 29% was quantified, in line with data obtained under DUV analyses, particularly by TELEMOS, which recorded a higher lignification in stressed fibres in response to abiotic stress. One must recall that both autofluorescence and biochemical analyses have the same limitation, i.e., values are calculated on signals including the middle lamellae surrounding the elementary fibres, describing then the bundle. Middle lamellae are known to be enriched in lignin (Lion et al., 2017) and can therefore cause an overestimation of the lignin content when speaking about elementary fibre in biochemical or fluorescence analyses.

Another important piece of information is obtained with the galactose/rhamnose (Gal/Rha) ratio, which is an indicator of ramification in the matrix and RG-I (Gorshkova and Morvan, 2006; Lefeuvre et al., 2018). In the present study, the Gal/Rha ratio calculated was 3.8 in the control fibres versus 2.8 in the stressed flax fibres. According to Lefeuvre *et al.* (2018), this lower ratio means that the ramification is less extended, arguably with a shorter galactose side chain length. Notably, long side galactose chains were purified from bast fibre G layer (Petrova et al., 2019).

Regarding the protein, despite the large standard deviation, the multispectral imaging showed a trend towards a higher content in the drought-stressed fibres, whereas the direct protein content quantified with the Dumas method clearly shows an increment of almost 50% in the stressed fibres.

Shives extracted from non-retted stems showed an increased amount of xylose in drought-stressed stems, while, unlike fibres, the amount of glucose barely changed between the two batches. Furthermore, a drastic decrease in the amount of lignin and protein in the xylem of drought-stressed stems compared to the control flax plants was observed.

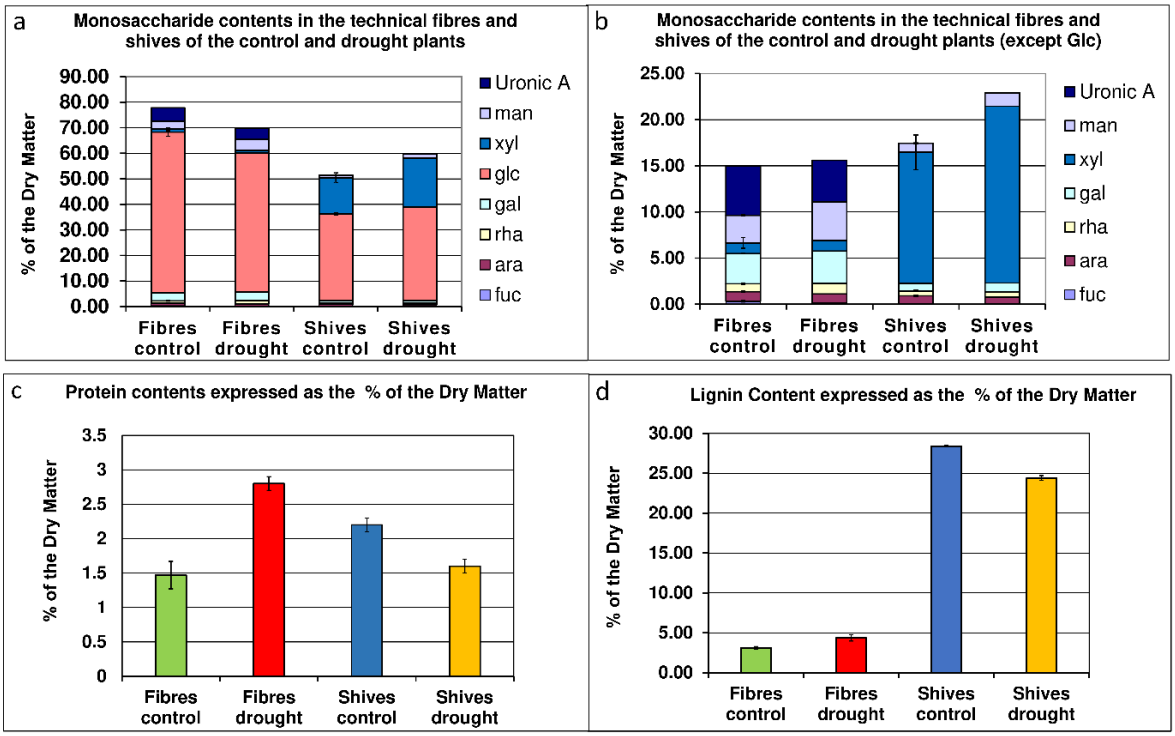

Figure 8. Biochemical analysis of monosaccharide with a) or without b) glucose, protein c) and lignin d) and content in fibres and shives (xylem). Values are given in % of dry mass. xyl: xylose; glc: glucose; gal: galactose; man: mannose; rha: rhamnose; ara: arabinose; fuc: fucose; and Uronic A: uronic acid.

Table 3. Detailed data of sugar analysis from fibres and shives. xyl: xylose; glc: glucose; gal: galactose; rha: rhamnose; ara: arabinose; fuc: fucose; and man: mannose. Gal/Rha and glucose/noncellulosic polysaccharide (NCP) ratios are also reported, SD standard deviation. All values are given in % of the dry mass.

FIBRES											
%	**fuc**	**ara**	**rha**	**gal**	**glc**	**xyl**	**man**	**Uronic Acid**	**total sugars**	**Gal / Rha**	**Glc / NCP**
Control	0.31	1.06	0.85	3.27	62.8	1.17	2.99	5.32	77.8	3.84	6.5 : 1
SD	0.17	0.04	0.59	0.26	1.85	0.13	0.03	0.80	3.81	-	-
Drought stress	0.11	1.00	1.18	3.36	54.3	1.17	4.17	4.50	69.9	2.86	4.9 : 1
SD	0.00	0.11	0.12	0.16	0.34	0.11	0.03	0.28	0.21	-	-
SHIVES											
Control	0.06	0.85	0.53	0.82	33.95	14.22	0.98	/	51.40	/	/
SD	0.00	0.07	0.07	0.03	0.43	1.89	0.04	/	1.66	/	/
Drought stress	0.04	0.73	0.58	0.95	36.71	19.15	1.45	/	59.62	/	/
SD	0.08	0.06	0.10	0.02	1.63	0.59	0.07	/	2.43	/	/

Direct quantification of some hydroxycinnamic acids linked in the cell wall by ester bridges has been performed on technical fibres and shives (**Table 4**). This quantification includes ferulic acid as a form of monomer (major component) or one dimer (the 8–5' benzofuran) and both coumaric and sinapic acids. A slight increase in

FA, sinapic and *p*-coumaric acids can be monitored in bast fibre from the drought-stressed plants and a decrease in *o*-coumaric acid. No traces of dimer of 8–5' ferulic acid dimer can be found in technical fibres. For shives, *o*-coumaric acid was not detected, and a dimer of 8–5' ferulic acid was quantified in a similar amount in the drought and control plant shives. A general slight decrease is observed in ferulic acid, *p*-coumaric and sinapic acids in drought plant shives.

Table 4. Amounts of hydroxycinnamics (monomers and dimer) released by mild alkaline hydrolysis of the control and drought technical fibres and shives. Values are expressed as % of dry matter. FA-E: ferulic acid in E or Z isomers; pCA: coumaric acid; oCA: o-coumaric acid; SA: sinapic acid; and DiFA8–5'C 8,5'-DiFerulic acid benzofuran form. DM is the dry matter.

	in % of the DM	FA-E	pCA	SA	oCA	DiFA8-5'C
Technical fibres	**Control**	1.5×10^{-5}	1.4×10^{-5}	1.6×10^{-6}	2.7×10^{-6}	0
	SD	1.6×10^{-6}	5.4×10^{-7}	$8{,}5\times10^{-8}$	1.4×10^{-7}	0
	Drought	1.9×10^{-5}	2.1×10^{-5}	1.8×10^{-6}	7.0×10^{-7}	0
	SD	5.9×10^{-7}	1.1×10^{-6}	$1{,}2\times10^{-7}$	1.3×10^{-7}	0
Shives	**Control**	3.6×10^{-5}	3.3×10^{-5}	2.5×10^{-6}	0	5.3×10^{-7}
	SD	1.8×10^{-6}	2.4×10^{-6}	1.2×10^{-7}	0	1.3×10^{-7}
	Drought	1.7×10^{-5}	2.2×10^{-5}	1.2×10^{-6}	0	6.4×10^{-7}
	SD	2.7×10^{-7}	3.5×10^{-8}	7.1×10^{-8}	0	1.8×10^{-7}

Table 5. NMR data**.** Relaxation times associated with C_4 phase areas for control and drought-stressed samples, $T_{1\rho}^{H}$ is the spin lattice in the rotating frame relaxation times for protons. Crystallinity index (CI), LFD and LFAD are the crystallinity ratios obtained from the C_4 and C_6 region deconvolution of ^{13}C CP/MAS spectra, the lateral fibril dimension, the lateral fibril aggregate dimension and the hemicellulose content, respectively.

	$T_{1\rho}^{H}$ (ms)	
	Control	**Drought**
C_4	20	36
	^{13}C CP/MAS	
Crys C_4(%)	57	55
LFD (nm)	4.6	4.5
LFAD (nm)	20	19.2

In addition to biochemical quantifications, ssNMR investigations were conducted. Flax fibres from the two batches did not show differences in crystalline cellulose content under NMR analysis, with a value of approximately 55–57%; however, the Nuclear Magnetic Relaxation Time Analyses $T_{1\rho}^{H}$ demonstrated a higher value of almost 50% in fibres extracted from drought-stressed plants compared to that of control samples. This value is due to the molecular organisation in the range of a few nanometres (2–30 nm)

around the cellulose fibres, and a higher value in drought-stressed fibres could suggest a more organised structure in components other than crystalline cellulose, i.e., pectin or hemicellulose (**Table 5**) which appeared altered in the drought-stressed fibres, as discussed above. However, at the ultrastructural level, the cellulose LFD and LFAD parameters, representing the size parameters of both cellulose fibril and fibril aggregates, remained on the same order for both the control and drought-stressed fibres.

4.4. Impact of drought on fibres and cell wall mechanical properties

Mechanical properties were investigated at the single fibre scale by tensile testing but also at the cell wall scale by AFM PF-QNM and NI. **Table 6** shows the tensile properties obtained on the two batches of fibres as well as the number and diameters of the fibres considered.

Table 6. Diameters and tensile properties of tensile tested flax fibres.

	Number of fibres	Diameter (µm)	Young's Modulus (GPa)	Strength at break (MPa)	Elongation at break (%)
Control	58	19.5±4.7*	48.3±20.2 n.s.	1160±548 n.s.	2.45±0.64 n.s.
Drought stressed	58	16.3±3.6*	54.4±22.8 n.s.	1180±503 n.s.	2.28±0.63 n.s.

* statistically significantly different ($p<0.5$), n.s.= not significant

Previous results showed that drought stress has a clear impact on flax fibre biochemical content but also on their morphology. The diameters measured under an optical microscope on approximately 60 fibres demonstrated a significant difference ($p < 0.5$) between the control (19.3 ± 4.4 µm) and drought-stressed fibres (16.1 ± 3.5 µm), tested using Welch's t-test. However, neither the morphology nor the biochemical modifications seem to affect the longitudinal mechanical properties, which are still comparable between the two batches. Interestingly, these mechanical performances are fully in line with literature data collected on 50 batches of single flax fibres (Baley and Bourmaud, 2014), characterised with the same protocol and equipment in the same lab (**Figure 9**); our batches have an average Young's modulus very similar to the average value of these 50 batches of elementary fibres and a strength at break slightly higher.

Thus, at the elementary fibre scale, the tensile properties were not significantly affected, and they maintained their potential as composite material reinforcement, although the crop yield of the fibres extracted from the stressed plants was drastically reduced; this stability of flax fibre mechanical performance has already been demonstrated on a panel of 4 varieties with significantly different fibre yields (Goudenhooft et al., 2017).

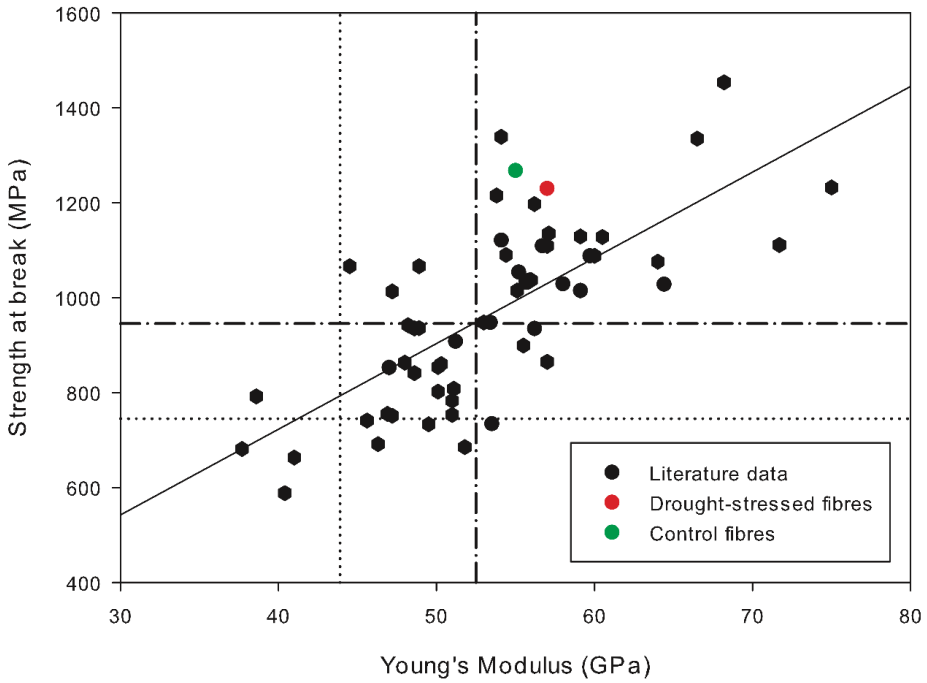

Figure 9. Comparison of the tensile Young's modulus and strength at break of the control and stressed flax fibres with literature data (Baley and Bourmaud, 2014).

At the cell level, the topography and indentation modulus obtained by AFM of fibres from control and stressed batches are reported in **Figure 10**. The average indentation modulus obtained by AFM PF-QNM in control flax fibres was 19.3 ± 1.4 GPa and 19.0 ± 1.4 GPa in drought-stressed fibres, resulting in a nonsignificant difference (p value > α), without any mechanical gradient in the G or S_1 layers in both cases. In light of the significant biochemical variations between the control and drought samples, this lack of contrast in indentation modulus emphasizes the hypothesis of a compensation effect of the plant metabolism to maintain its internal mechanical specifications in accordance with the *in planta* function. Further experiments run with nanoindentation confirmed the results obtained by AFM with an average indentation modulus of 19.1 ± 3.5 GPa and 19.5 ± 2.7 GPa obtained for control and drought-stressed fibres, respectively, with again a nonsignificant difference (p value > α).

This stability in the indentation modulus, obtained by both nanoindendation and AFM tests, provides pertinent indications of a poor evolution of both cellulose macrofibrils (crystallinity and MFA) and possible moderate changes in the polysaccharidic matrix ultrastructure, which can impact the transverse and shearing cell wall properties and, consequently, the indentation modulus. Conversely, the hardness (H) measured is contrasted, being statistically significant between drought-stressed and control fibres (341 ± 34 MPa in stressed fibres against 296 ± 35 MPa in control), with a clear higher hardness recorded in the drought fibres (**Table 7**). Gindl *et al.* (2002) and Stanzl-Tschegg *et al.* (2009) have evidenced that the hardness of plant cell walls is a good indicator of noncellulosic polymer evolution; here, hardness measurements confirm the biochemical changes, which has been shown to be more sensitive than the indentation modulus to highlight matrixial changes.

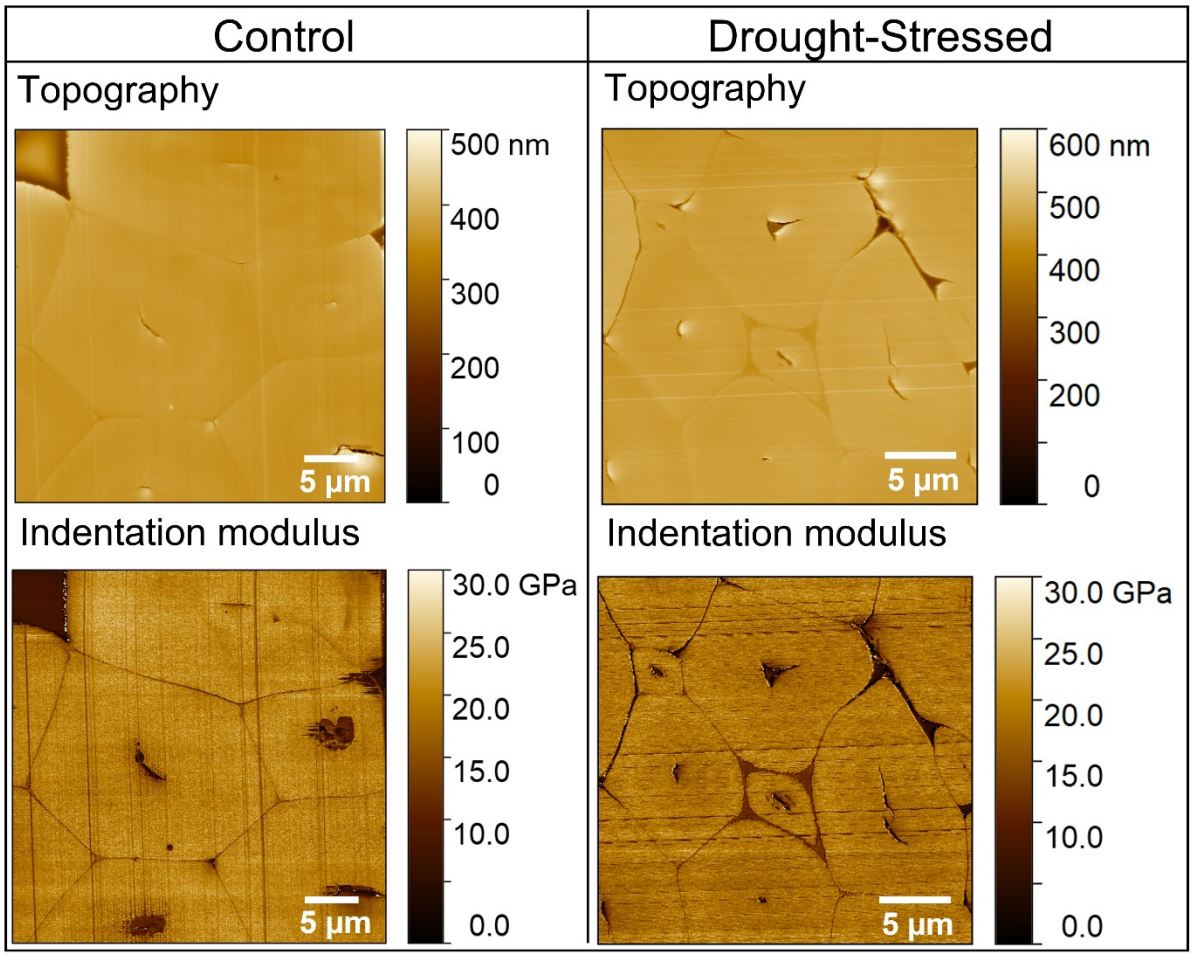

Figure 10. Indentation modulus mapping and topography of control and drought-stressed flax cell walls obtained by AFM PF-QNM experiments.

Table 7. Mean values of indentation modulus and hardness recorded by AFM and nanoindentation.

Characterisation technique	Control	Drought-stressed
AFM PF-QNM		
Indentation Modulus (GPa)	19.3±1.4 n.s.	19.0±1.4 n.s.
Nanoindentation		
Indentation Modulus (GPa)	19.1±3.5 n.s.	19.5±2.7 n.s.
Hardness (MPa)*	296±35*	341±34*

* statistically significant (p-value <0.5)

5. Discussion

All the results obtained in this work are summarised in Table 8.

Table 8. Summary table of observations divided by techniques.

Flax plant DAMARA variety (2019)	**Drought-stressed (Fourches)**	
Rainfall	<100 mm cumulated rainfall	
Height (mm)	59.0 ±6.5 **(- 28%)** *	
Technical fibre Yield	13.8% **(-14 %)** *	
DUV imaging	**Fibers** Proteins: + (n.s.) Phenolic: + (n.s.) Lignin: +*	**Xylem** Proteins: +* Phenolic: + (n.s.) Lignin: +*
DUV microspec.	**Fibres** Prot.: less intense, less homogeneous PC: more intense, well distributed Lignin: /	**Xylem** Prot.: less intense, less homogeneous PC: more intense, well distributed Lignin: n.s.
Total Monosaccharides * (% dry mass)	**Fibres** 69.89±0.21 **(-10%)** (Glc= -13%, Man= +28%)	**Xylem** 59.62±2.43 **(+14%)** (Xyl= +26%, Man= +33%)
Lignin * (% dry mass)	**Fibres** 4.37±0.40 **(+29%)**	**Xylem** 24.4±0.30 **(-14%)**
Protein * (% dry mass)	**Fibres** 2.8±0.1 **(+47%)**	**Xylem** 1.6±0.1 **(-27%)**
Hydroxycinnamic *	**Fibres** **+12%/+30%** (except oCA= -74%)	**Xylem** **-35%/-50%** (except DFA8-5C= +17%)
^{13}C NMR CP/MAS		
Crys C_4 (%)	55% (n.s.)	
LFD **&** LFAD	4.5 (n.s.); 19.2 (n.s.)	
^{13}C VCT-CP/MAS	$\mathbf{T}_{1\rho}^{H}$ **= +45-50% ***	
Diameter fibres (µm)	16.1 **(-17%)** *	
Tensile test		
Young's modulus (GPa)	54.4±22.8 (n.s.)	
Strength at break (MPa)	1180±503 (n.s.)	
AFM PF-QNM		
Indentation Modulus (GPa)	19.0±1.4 (n.s.)	
Nanoindentation		
Indentation Modulus (GPa)	19.5±2.7 (n.s.)	
Hardness (MPa)	341±34 *** (+13%)**	

*= statistically significantly different (p<0.5), n.s= not significantly different

Flax plants grown under drought conditions have undergone important modifications in terms of morphology, as indicated by a reduction of both the height and stem diameters. This was already observed for linseed by Kariuki *et al.* (Kariuki et al., 2016), who also documented an important decrease in the number of leaves under water stress.

Abot *et al.* studied *Cannabis sativa* under water stress conditions and recorded a delay in stem maturity for stressed stems (Abot et al., 2013). Conversely, it was observed that other plants anticipated their maturity by trying to shorten their growing cycle to prevent drought stress during critical periods, such as flowering (Farooq et al., 2012; McMaster and Wilhelm, 2003). In drought-stressed flax plants, it was observed delays in flowering and maturation (not shown in this paper). In order to assess if the drought condition has physiologically induced suffering of plant, the ^{13}C stable isotope abundance has been use in this study because it has been widely utilized to deliver useful information about leaf gas exchanges and photosynthetic capacities. Photosynthetic carbon discrimination comes from two main steps during CO_2 fixation in C3 plants : at first a small isotopic discrimination (4,4°/₀₀) caused by CO_2 diffusion from the atmosphere to the leaf photosynthetic cells and 2) a strong isotope effect (29°/₀₀) associated with ribulose 1,5-bisphosphate carboxylase/oxygenase (RuBisCO) carboxylation, which preferentially uses ^{12}C relative to ^{13}C (Farquhar et al., 1989). Under low-water diet, the decreased of stomatal conductance and photosynthetic CO^2 fixation lead to an increase in $\delta^{13}C$, reflecting that plants are indeed suffering from drought stress (Souza Mateus et al., 2021). The stronger increase in fiber $\delta^{13}C$ could reflect metabolic isotope discriminations in cellulose synthesis, which is generally ^{13}C-enriched compared to photosynthetically fixed carbon (Gleixner et al., 1993 ; Schmidt & Gleixner, 1998 ; Kodina, 2010), and this effect could be reinforced by post-photosynthetic isotope fractionations during biomass synthesis (such as for rhamnose) and/or respiratory CO_2 loss that could increase under stress conditions (Badeck et al., 2005 ; Cernusak et al., 2009 ; Flexas et al., 2005).

Under drought stress, it is known that flax plants reduce their fibre diameter, and both the fibre number and length are affected (Chemikosova et al., 2006). This fact, together with the reduced height and diameter of the plant, has a direct impact on the fibre yield and can explain the lower fibre yield obtained from drought-stressed plants (13% versus 17% under normal conditions, and approximately 20–28% in the literature). A similar loss of yield was already reported in Lefeuvre *et al.* for drought-stressed stems of the Marylin flax variety (Lefeuvre et al., 2018).

Histochemical analysis with phloroglucinol demonstrated a slight colouring of flax fibres from the two batches, but no differences between the drought and control fibres were detected in their cell walls or in their middle lamellae, where lignin is arguably mainly present (Richely et al., 2021).

Lignin is a complex polyphenolic constituent of different monolignols with the role of providing stiffness to the plant as a mechanical function as well as hydrophobicity (Neutelings, 2011) and, in the case of stress, serving as encrusting polymers with the aim of increasing the resistance of plants to unfavourable environments. Indeed, hyperlignification was also observed in the growth of other plant species under drought stress (Frei, 2013; Malavasi et al., 2016), and a role of a physical barrier was observed in stressed maize leaves, where higher lignification was attributed to the plant response to limit water transpiration (Hu et al., 2009). However, hyperlignification due to stress is not systematic in all tissues of the plant, and it also differs among the plant species investigated (Cabane et al., 2012). Nevertheless, since the lignin content in flax fibres is very low, it is difficult to link the presence of lignin to the stiffness of the cell wall. Thanks to UV fluorescence analysis and direct biochemical quantification, it was possible to deeply investigate proteins (especially tyrosine and tryptophan) and hydroxycinnamic acids. Tyrosine and tryptophan are amino acids belonging to protein

and are essential for plant metabolism. Indeed, tyrosine, as a tyrosine phosphorylation, is linked to the capacity of cell division, which is reduced when the plant undergoes drought conditions (Schuppler et al., 1998; Bartels and Sunkar, 2005). Furthermore, protein tyrosine phosphatase is a negative regulator of the phytohormone abscisic acid (ABA), which is responsible for the movement of stomata and, under drought stress, induces their closure (Bartels and Sunkar, 2005; Shankar et al., 2015). Tryptophan is an amino acid used for the synthesis of protein and other compounds with a different role in plant growth, resistance and reproduction; in particular, it is the precursor of auxin biosynthesis, a hormone directly linked to growth capacity (Sihel, 1998; Zhao, 2010). Extensive research on wheat growth under drought stress conditions showed that plants had an increase in both tryptophan and tyrosine in their leaves (Bowne et al., 2012).

A large increase in tyrosine and tryptophan was also observed for tree stems of elm and oak wood species subjected to moderate to extremely severe drought conditions (Rodríguez-Calcerrada et al., 2021).

Hydroxycinnamic acids are well known to be antioxidants (Chen and Ho, 1997), and their biosynthesis directly involves tyrosine and phenylalanine, which are their precursors (Macoy et al., 2015; El-Seedi et al., 2018). At the same time, lignin is biosynthesised from hydroxycinnamic acids (Humphreys and Chapple, 2002; Hoffmann et al., 2004). In flax plants, hydroxycinnamic acids play several roles, such as cross-linking and mechanical support, and are directly involved in the plant response to biotic and abiotic stress. (Gorshkova et al., 2000). Most likely, for these reasons, other teams found that the amount of hydroxycinnamic acids seems to increase when plants grow under drought stress (Macoy et al., 2015; Šamec et al., 2021).

In general, the cutin and waxes in the external part of leaves and stems of plants, which can generate autofluorescence (Verhertbruggen et al., 2017), are partially responsible for water transpiration, and their thickness seems to increase with drought, as in the case of tea leaves (Chen et al., 2020).

In the epidermis of drought-stressed flax stems examined here, a slightly higher fluorescence intensity of lignin was observed than that in control stems, while the fluorescence intensity of protein and hydroxycinnamic acids tended to decrease (**Figures 6.e, f** and **7**).

In cortical parenchyma, the difference in thickness was evident and apparently higher in the stressed stems with also larger cells, as one can note in **Figures 6.a-d**. Control stems, on the contrary, had a dense, thin and more compact cortical parenchyma. In terms of molecular distribution, high variability was found in the cortical parenchyma of the control, while the stressed stems showed a more homogeneous response in all three stems investigated, especially regarding tyrosine and tryptophan (**Figures 6.e, f**). As in cortical parenchyma, phloem showed extremely high variability in controlled plants, while the standard deviation was reduced in the stressed stems. Unfortunately, in the literature, there is a lack of information regarding the response of these tissues to drought stress. The greatest differences between the two flax batches were found in the xylem and fibres. In the xylem, it was observed an increase in fluorescence intensity in all three filters for the stressed stems, especially for the filter assigned to

protein (327–353) and lignin (480–550), as reported in **Figures 6.e, f**. This seems to be in line with the literature because a higher xylem lignification appears to be beneficial for drought-stressed plants of other species (Cabane et al., 2012; Frei, 2013; Malavasi et al., 2016). However, to the best of our knowledge, there is no literature on flax xylem lignification under drought stress.

Nevertheless, UV fluorescence results were contradicted by direct biochemical quantification, where a lower content of protein, lignin and hydroxycinnamic acids was measured in drought xylem than in the control flax plants (**Tables 4** and **Figures 8.c, d**). A hypothesis to explain this discrepancy relies on the method of quantification.

The specificity of the fluorescence of lignin has already been questioned (Beaugrand et al., 2022; Vidot et al., 2019), and a hypothesis is that nonlignin molecules capable of fluorescing in the range of 480–550 nm may have overestimated the lignin amount by the autofluorescence method. On the other hand, the direct method of quantification can be influenced by the contrasting affinity of reagents with fine molecule structures. For instance, lignin quantification by acetyl bromide may be sensitive to the lignin ratio of G/H and S monomers, and when lignin is stained by phloroglucinol (Day et al., 2005) in flax, it shows a contrasting location and distribution compared to safranin-based quantification (Baldacci-Cresp et al., 2020). Quantification for accurate and specific measurements of complex structures is still a challenge.

Similar limitations of both techniques were also observed for the quantification of protein and hydroxycinnamic acids. Deep UV fluorescence investigations allow the detection of only a few amino acids capable of fluorescing, such as tryptophan, while the biochemical method is based on the quantification of all the azote contents of the sample and reflects all 20 amino acids constituting proteins. Thus, if the draught samples have a high protein content but are not enriched in aromatic amino acids that can fluoresce, then DUV imaging may underestimate the real amount of protein.

In stressed xylem, for example, the biochemical quantification approach also recorded a lower amount of protein than the control one (**Figure 8c**). It is possible to conclude that although drought stress could have caused an enrichment in tryptophan and tyrosine in the xylem observed under fluorescence, the overall amount of protein calculated by direct quantification, therefore also considering nonaromatically enriched amino acids, probably decreased.

Contrary to protein, for the analysis of hydroxycinnamic acids, direct quantification can only quantify ester bonds, and only certain forms, but does not exhaustively quantify all hydroxycinnamics. For this reason, in this case, DUV quantification is certainly more representative of the overall hydroxycinnamic acids if the two methods are compared.

Regarding flax fibres, under DUV light, a higher fluorescence intensity for all three filters was recorded in stressed flax fibres (**Figures 6.e, f**) and fluorescence microspectroscopy clearly shows enrichment, especially in hydroxycinnamic acids **(Figure 7**). The higher amounts of protein, hydroxycinnamic acids and lignin were confirmed by direct quantification (**Figures 8.c, d** and **Table 4**). An increase in lignin was expected in response to drought stress, as already reported in the literature for both flax and hemp fibres (Abot et al., 2013; Lefeuvre et al., 2018), but no literature data have been found on protein and hydroxycinnamic acids.

Monosaccharides were also investigated and linked to cellulose and hemicellulose. Biochemical analysis by wet chemistry (GC-FID) also demonstrated a moderate decrease in glucose content for stressed flax, probably compensating for the biosynthesis of mannose, whose content increased. In extracted drought-stressed flax fibres, Lefeuvre *et al.* found more xylan as a structured polysaccharide and a decrease in gel/matrix polysaccharides (rhamnogalacturonan and homogalacturonan), a decrease in uronic acid, a decrease in the Gal/Rha ratio and a decrease in total sugars extracted in acid compared with control flax fibres (Lefeuvre et al., 2018). The presented results are generally in line with their observations (**Figures 1.a, b** and **Table 3**), and a lower Gal/Rha ratio in drought-stressed fibres means a modification in the RG-I polymer responsible for the order of the microfibril network (Chemikosova et al., 2006).

Increased quantities of mannose and galactose were observed by Bowne *et al.* in leaf tissues of wheat growth under drought conditions, and the authors hypothesised that mannose and galactose are correlated with plant defence in an attempt to avoid loss of water in unfavourable environmental conditions (Bowne et al., 2012). This may also be a valid explanation in the case of flax fibres.

Table 9. Flax fibre cell wall layers and approximative composition readapted from (Gorshkova et al., 2018a, 2018b; Goudenhooft et al., 2019)

Fibre cell wall layer	Approximative composition
PW	~ 25-40% Cellulose ~ 30% Hemicellulose (xyloglucan and less amount of arabinoxylan) ~ 30% Pectins (homogalacturonan and less amount of RG-I, RG-II and arabinogalactan)
S1	~ 30-50% Cellulose ~ 25% Hemicellulose (mainly xylan, xyloglucan and a small amount of glucomannans) ~ 5% Pectins (homogalacturonan) ~ 20-30% Lignin
G	~ 75-90% Cellulose ~ 5-10% Pectins (mainly RG-I, probably also a small amount of homogalacturonan) Small amount of glucomannans and arabinogalactans

Rihouey *et al.* reported on flax fibres that mannose is currently known only in the form of glucomannans and that glucomannans play a main structural role in fibre cells I (Rihouey et al., 2017). In the present study, mannose was the main monosaccharide that changed between the two batches and became more abundant in the drought-stressed fibres. Because mannose content is extremely low in both lots compared to glucose and glucomannans are mainly located in the G layer (Gorshkova et al., 2018a, 2018b; Goudenhooft et al., 2019), as illustrated in **Table 9**, the stressed flax fibres are apparently enriched in glucomannans.

The amount of glucose, on the other hand, decreases in drought-stressed fibres and the xyloglucan content first, which are calculated with the ratio Glc/Xyl=1.5 with the rest of glucose after the estimation of glucomannans (Rihouey et al., 2017), and xylans then, which are calculated with the remaining xylose content (Rihouey et al., 2017), probably decrease as well because in both batches investigated here, the xylose is constant.

Thus, hemicelluloses in the S_1 layer are particularly reduced in drought-stressed fibres and probably partially replaced by other molecules, such as lignin, protein and hydroxycinnamic acids.

Regarding pectins, using the Gal/Rha ratio, it was found that drought-stressed fibres had a smaller ratio and, consequently, the stressed fibres had RG-I with shorter galactan chains (Gorshkova and Morvan, 2006; Lefeuvre et al., 2018). This result confirms the results obtained by Lefeuvre *et al.* (Lefeuvre et al., 2018), who observed the same smaller ratio in drought-stressed flax fibres than in the controls.

Despite all these important biochemical modifications at the stem and fibre levels, the mechanical properties of flax fibres in terms of both indentation measured at the nanoscale level and Young's moduli measured by tensile testing were preserved, and stressed and control fibre mechanical properties were comparable at both the local and fibre scales (**Figures 9** and **10**). Our results are in agreement with the study of Lefeuvre *et al.*, where batches of flax fibre growth under drought and control conditions were measured by tensile testing, and the authors did not observe any significant differences (Lefeuvre et al., 2014). It can be argued that tensile test behaviour and properties are mainly driven by cellulose content and arrangement due to the poor MFA and high crystalline cellulose content of falx fibres; consequently, changes in the polysaccharidic matrix are not easily perceptible with this method.

In fact, in the present study, thanks to the NMR analysis, it was observed that the crystallinity index was the same as the microfibril network between the two batches (**Table 5**), which can explain why the longitudinal mechanical properties of the fibres measured by the single fibre tensile test were quite the same, except for the hardness.

Hardness measured by nanoindentation was higher in the drought-stressed fibres than in the control fibres. Eder *et al.* reported that hardness is mainly due to the matrix behaviour of the fibre cell (Eder et al., 2013). Indentation is a much more complex loading that leads to the fact that the indentation modulus depends on the longitudinal Young's modulus but also to the transverse and shear moduli (Jäger et al., 2011). Hence, indentation modulus is sensitive to the cellulose microfibrils elastic properties, such as the longitudinal Young's modulus, but also to the cell wall matrix viscoelastic properties. Despite the changes in the chemical composition and organisation of the matrix observed here, this modulus is not significantly altered. Conversely, the hardness measured by nanoindentation was higher in drought-stressed fibres than in control one. Eder *et al.* reported that the hardness is mainly due to the matrix viscoplastic (irreversible) behaviour of the cell wall (Eder et al., 2013). Similar trends were addressed by Gindl *et al.* (2002) and Stanzle-Tschegg *et al.* (2009), by comparing lignification of spruce tracheids for different maturity degrees and thermally treated wood, respectively.

The longitudinal elastic modulus and strength are due to the crystalline cellulose and are unchanged as well as the indentation modulus, which depends on the viscoelastic properties of the cell wall matrix. Conversely, the hardness, which mainly depends on the viscoplastic properties of the cell wall matrix, varies between control and stressed fibres. Therefore, it can be hypothesised that biochemical changes would mainly impact the viscoplastic behaviour of the cell wall matrix.

Besides, the relationship between lignin and nanomechanical properties requires particular attention. The role of lignin in the mechanical properties of cell walls with cellulose microfibrils having a high microfibril angle has been deeply studied in wood, and a high lignin content has been observed to increase the shear modulus and strength of the matrix by filling the space between cellulose and hemicellulose (Özparpucu et al., 2019, 2017; Gindl et al., 2002), and the hardness measured resulted particularly sensible to the lignin concentration (Gindl et al., 2002).

Following the hypothesis in Rihouey *et al.* (2017), together with the observations done by Gindl *et al.* and Özparpucu *et al.* (2017, 2019), it is possible to hypothesise that: i) the higher amount of glucomannans and probably less branched RG-I in G layer, ii) the higher lignin content in S_1 layer and probably also iii) the lower Uronic Acid content (the more the Uronic Acid the more is the fibre strength (Bourmaud et al., 2013)) play a central role in the increased hardness of drought-stressed flax fibres helped to improve the hardness of drought-stressed flax fibres. However, the impact of homogalacturonans, protein and hydroxycinnamic acids on the fibre mechanical behaviour is still unclear.

6. Conclusion

The morphological, biochemical and mechanical properties of flax stems and fibres were explored after a severe drought. Particular attention was given to the study of single flax fibres because of their wide use in different industrial sectors and especially as composite material reinforcements.

Biochemical contrasts between the control and drought-stressed flax fibres were highlighted such as a huge increase in the protein and lignin content after drought stress, as well as an increase in hydroxycinnamates. Additionally, the morphology of the stems and fibres to be smaller in diameter than in control. The stiffness measures, ~~both~~ obtained through tensile and indentation tests, do not evolve with drought stress; these properties are mainly driven by cellulose arrangement and ultrastructure, which remain quite unchanged here. In contrast, indentation hardness confirms its role as a pertinent indicator of noncellulosic component changes. Thus, thanks to the stability of their mechanical properties at the fibre scale, fibres submitted to drought are still suitable for biocomposite and textile production, although their production yield drastically decreases.

Here, a flax variety rather tolerant to drought was selected, but future work will focus on flax varieties with a higher sensitivity to drought, such as the Aretha variety.

Acknowledgements

JB thanks Laurent Helary (INRAE, BIA) for technical assistance in the paraffin sectioning of the flax samples. JB thanks Lucas Demezet (INRAE, BIA) for the high skill in manually decorticating the flax stems and biochemical analysis. The authors wish to acknowledge the funding provided by the INTERREG IV Cross Channel program through the FLOWER project (Grant Number 23). Additionally, the authors wish to thank SOLEIL Synchrotron for funding the 20190064 proposal.

Supporting information

Supplementary data associated with this article can be found in the online version at doi:10.1016/j.indcrop.2022.115011.

References

Abot, A., Bonnafous, C., Touchard, F., Thibault, F., Chocinski-Arnault, L., Lemoine, R., Dédaldéchamp, F., 2013. Effects of cultural conditions on the hemp (Cannabis sativa) phloem fibres: Biological development and mechanical properties. J. Compos. Mater. 47, 1067–1077. https://doi.org/10.1177/0021998313477669

Akin, D.E., Gamble, G.R., Morrison III, W.H., Rigsby, L.L., Dodd, R.B., 1996. Chemical and Structural Analysis of Fibre and Core Tissues from Flax. J. Sci. Food Agric. 72, 155–165. https://doi.org/10.1002/(SICI)1097-0010(199610)72:2<155::AID-JSFA636>3.0.CO;2-X

ARVALIS Institut du végétal, 2019. Lin fibre: résultats et préconisations, Choisir & Décider. ARVALIS, Paris, France.

ARVALIS Institute du végétal, 2015. LIN FIBRE: Les activités d'ARVALIS institut du végétal au sein de la filière, Choisir & Décider. ARVALIS, Paris, France.

ASTM C1557-20, 2020. , Book of Standards Vol.15.01. ASTM International, West Conshohocken, PA. https://doi.org/10.1520/C1557-20

Audran, X., McLeod, L., 2011. France facing most severe drought in 50 years (No. FR9069). USDA foreign agricultural service.

Badeck FW, Tcherkez G, Nogues S, Piel C, Ghashghaie J. 2005. Post-photosynthetic fractionation of stable carbon isotopes between plant organs—a widespread phenomenon. Rapid Communications in Mass Spectrometry 19: 1381-1391.

Baldacci-Cresp, F., Spriet, C., Twyffels, L., Blervacq, A.-S., Neutelings, G., Baucher, M., Hawkins, S., 2020. A rapid and quantitative safranin-based fluorescent microscopy method to evaluate cell wall lignification. Plant J. 102, 1074–1089. https://doi.org/10.1111/tpj.14675

Baley, C., Bourmaud, A., 2014. Average tensile properties of French elementary flax fibers. Mater. Lett. 122, 159–161. https://doi.org/10.1016/j.matlet.2014.02.030

Barteau, G., Azoti, W., Gautreau, M., Francart, C., Alès, G., Jmal, H., Bouchet, J., Kervoëlen, A., Beaugrand, J., Bahlouli, N., Bourmaud, A., 2021. Recycling of wood-reinforced poly-(propylene) composites: A numerical and experimental approach. Industrial Crops and Products 167, 113518. https://doi.org/10.1016/j.indcrop.2021.113518

Bartels, D., Sunkar, R., 2005. Drought and Salt Tolerance in Plants. Crit. Rev. Plant Sci. 24, 23–58. https://doi.org/10.1080/07352680590910410

Beaugrand, J., Goudenhooft, C., Alvarado, C., Devaux, M.-F., Rivard, C., Durand, S., Chauvet, H., Réfrégiers, M., Jamme, F., Guillon, F., Baley, C., Bourmaud, A., 2022. Evolution of the flax cell wall composition during development and after gravitropism by synchrotron fluorescence imaging. Ind. Crops Prod. 175, 114256. https://doi.org/10.1016/j.indcrop.2021.114256

Bedigian, D., Harlan, J.R., 1986. Evidence for cultivation of sesame in the ancient world. Econ. Bot. 40, 137–154. https://doi.org/10.1007/BF02859136

Blakeney, B., Harris, P., Henry, R., Stone, B.A., 1983. A simple and rapid preparation of alditol acetates for monosaccharide analysis. Carbohydr. Res. 113, 291–299.

Bourmaud, A., Morvan, C., Bouali, A., Placet, V., Perré, P., Baley, C., 2013. Relationships between micro-fibrillar angle, mechanical properties and biochemical composition of flax fibers. Ind. Crops Prod. 44, 343–351. https://doi.org/10.1016/j.indcrop.2012.11.031

Bouvier d'Yvoire, M., Bouchabke-Coussa, O., Voorend, W., Antelme, S., Cézard, L., Legée, F., Lebris, P., Legay, S., Whitehead, C., McQueen-Mason, S.J., Gomez, L.D., Jouanin, L., Lapierre, C., Sibout, R., 2013. Disrupting the cinnamyl alcohol dehydrogenase 1 gene (BdCAD1) leads to altered lignification and improved saccharification in Brachypodium distachyon. Plant J. 73, 496–508. https://doi.org/10.1111/tpj.12053

Bowne, J.B., Erwin, T.A., Juttner, J., Schnurbusch, T., Langridge, P., Bacic, A., Roessner, U., 2012. Drought Responses of Leaf Tissues from Wheat Cultivars of Differing Drought Tolerance at the Metabolite Level. Mol. Plant 5, 418–429. https://doi.org/10.1093/mp/ssr114

Cabane, M., Afif, D., Hawkins, S., 2012. Lignins and Abiotic Stresses, in: Advances in Botanical Research. Elsevier, pp. 219–262. https://doi.org/10.1016/B978-0-12-416023-1.00007-0

Cernusak LA, Tcherkez G, Keitel C, Cornwell WK, Santiago LS, Knohl A, Barbour MM, Williams DG, Reich PB, Ellsworth DS. 2009. Why are non-photosynthetic tissues generally 13C enriched compared with leaves in C3 plants? Review and synthesis of current hypotheses. Functional Plant Biology 36: 199-213.

Chemikosova, S.B., Pavlencheva, N.V., Gur'yanov, O.P., Gorshkova, T.A., 2006. The effect of soil drought on the phloem fiber development in long-fiber flax. Russ. J. Plant Physiol. 53, 656–662. https://doi.org/10.1134/S1021443706050098

Chen, J.H., Ho, C.-T., 1997. Antioxidant Activities of Caffeic Acid and Its Related Hydroxycinnamic Acid Compounds. J. Agric. Food Chem. 45, 2374–2378. https://doi.org/10.1021/jf970055t

Chen, M., Zhu, X., Zhang, Y., Du, Z., Chen, X., Kong, X., Sun, W., Chen, C., 2020. Drought stress modify cuticle of tender tea leaf and mature leaf for transpiration barrier enhancement through common and distinct modes. Sci. Rep. 10, 6696. https://doi.org/10.1038/s41598-020-63683-4

Crops and livestock products: flax fibre and tow [WWW Document], 2021. . FAOSTAT. URL www.fao.org (accessed 8.16.21).

Day, A., Ruel, K., Neutelings, G., Crônier, D., David, H., Hawkins, S., Chabbert, B., 2005. Lignification in the flax stem: evidence for an unusual lignin in bast fibers. Planta 222, 234–245. https://doi.org/10.1007/s00425-005-1537-1

Devaux, M.-F., 2018. Synchrotron Time-Lapse Imaging of Lignocellulosic Biomass Hydrolysis: Tracking Enzyme Localization by Protein Autofluorescence and Biochemical Modification of Cell Walls by Microfluidic Infrared Microspectroscopy. Frontiers in Plant Science 9, 16.

Eder, M., Arnould, O., Dunlop, J.W.C., Hornatowska, J., Salmén, L., 2013. Experimental micromechanical characterisation of wood cell walls. Wood Sci. Technol. 47, 163–182. https://doi.org/10.1007/s00226-012-0515-6

El-Seedi, H.R., Taher, E.A., Sheikh, B.Y., Anjum, S., Saeed, A., AlAjmi, M.F., Moustafa, M.S., Al-Mousawi, S.M., Farag, M.A., Hegazy, M.-E.F., Khalifa, S.A.M., Göransson, U., 2018. Hydroxycinnamic Acids: Natural Sources, Biosynthesis, Possible Biological Activities, and Roles in Islamic Medicine, in: Studies in Natural Products Chemistry. Elsevier, pp. 269–292. https://doi.org/10.1016/B978-0-444-64068-0.00008-5

European Environment Agency, 2019. Climate change adaptation in the agriculture sector in Europe. Publications Office, LU.

Farooq, M., Hussain, M., Wahid, A., Siddique, K.H.M., 2012. Drought Stress in Plants: An Overview, in: Aroca, R. (Ed.), Plant Responses to Drought Stress. Springer Berlin Heidelberg, Berlin, Heidelberg, pp. 1–33. https://doi.org/10.1007/978-3-642-32653-0_1

Farquhar, G.D., O'Leary, M.H., Berry, J.A., 1982. On the relationship between carbon isotope discrimination and the intercellular carbon dioxide concentration in leaves. Aust. J. Plant Physiol. 9, 121–137

Flexas J, Galmes J, Ribas-Carbo M, Medrano H. 2005. The Effects of Water Stress on Plant Respiration. Plant respiration in Advances in Photosynthesis and Respiration book series (AIPH,volume 18) pp85-94. Lambers & Ribas Carbo Eds, Springer New-York (USA).

Frei, M., 2013. Lignin: Characterization of a Multifaceted Crop Component. Sci. World J. 2013, 1–25. https://doi.org/10.1155/2013/436517

Gao, C., Sheteiwy, M. S., Han, J., Dong, Z., Pan, R., Guan, Y., . . . Hu, J. (2020). Polyamine biosynthetic pathways and their relation with the cold tolerance of maize (Zea mays L.) seedlings. Plant Signaling & Behavior, 15(11), 1807722.

Gindl, W., Gupta, H.S., Grünwald, C., 2002. Lignification of spruce tracheid secondary cell walls related to longitudinal hardness and modulus of elasticity using nano-indentation. Can. J. Bot. 80, 1029–1033. https://doi.org/10.1139/b02-091

Giuliani, A., Jamme, F., Rouam, V., Wien, F., Giorgetta, J.-L., Lagarde, B., Chubar, O., Bac, S., Yao, I., Rey, S., Herbeaux, C., Marlats, J.-L., Zerbib, D., Polack, F., Réfrégiers, M., 2009. DISCO: a low-energy multipurpose beamline at synchrotron SOLEIL. J. Synchrotron. Rad. 16, 835–841. https://doi.org/10.1107/S0909049509034049

Gleixner G, Danier HJ, Werner RA, Schmidt HL. 1993. Correlations between the 13C content of primary and secondary plant products in different cell compartments and that in decomposing basidiomycetes. Plant physiology 102: 1287-1297.

Gomez-Campos, A., Vialle, C., Rouilly, A., Sablayrolles, C., Hamelin, L., 2021. Flax fiber for technical textile: A life cycle inventory. J. Clean. Prod. 281, 125177. https://doi.org/10.1016/j.jclepro.2020.125177

Gorshkova, T., Chernova, T., Mokshina, N., Ageeva, M., Mikshina, P., 2018a. Plant 'muscles': fibers with a tertiary cell wall. New Phytol. 218, 66–72. https://doi.org/10.1111/nph.14997

Gorshkova, T., Mikshina, P., Petrova, A., Chernova, T., Mokshina, N., Gorshkov, O., 2018b. Plants at Bodybuilding: Development of Plant "Muscles," in: Plant Biomechanics: From Structure to Function at Multiple Scales. Springer, Cham, pp. 141–163. https://doi.org/10.1007/978-3-319-79099-2_7

Gorshkova, T., Morvan, C., 2006. Secondary cell-wall assembly in flax phloem fibres: role of galactans. Planta 223, 149–158. https://doi.org/10.1007/s00425-005-0118-7

Gorshkova, T., Salnikov, V.V., Pogodina, N.M., Chemikosova, S.B., Yablokova, E.V., Ulanov, A.V., Ageeva, M.V., van Dam, J.E.G., Lozovaya, V.V., 2000. Composition and Distribution of Cell Wall Phenolic Compounds in Flax (Linum usitatissimum L.) Stem Tissues. Ann. Bot. 85, 477–486. https://doi.org/10.1006/anbo.1999.1091

Goudenhooft, C., Bourmaud, A., Baley, C., 2019. Flax (Linum usitatissimum L.) Fibers for Composite Reinforcement: Exploring the Link Between Plant Growth, Cell Walls Development, and Fiber Properties. Front. Plant Sci. 10, 411. https://doi.org/10.3389/fpls.2019.00411

Goudenhooft, C., Bourmaud, A., Baley, C., 2017. Varietal selection of flax over time: Evolution of plant architecture related to influence on the mechanical properties of fibers. Ind. Crops Prod. 97, 56–64. https://doi.org/10.1016/j.indcrop.2016.11.062

Goulard, A., Agria Grand Est, APM, Bâtir en balles, Blackbird, Culture In, Dedienne Multiplasturgy, Egide, Focal, LabelBreed, Notox, S.Randé/CELC, Comité Champagne, Chambre d'Agriculture de l'Aube, Construire en Chanvre, Culture in Varian, FBT Isolation, NatUp fibres, Faurecia, France Miscanthus, FRD, InterChanvre, Parexlanko, Pixabay, 2020. Mémento 2020: Panorama des marchés Fibres végétales techniques en matériaux (hors bois) en France.

Habets, F., Viennot, P., 2015. Évolutions constatées et prévi-sibles des principales composantes du climat ayant un effet sur l'agriculture avec un focus sur l'hydrologie, in: Changement Climatique et Agriculture: Comprendre et Anticiper, Ici et Ailleur. pp. 24–32.

Hatfield, R., Fukushima, R.S., 2005. Can Lignin Be Accurately Measured? Crop Sci. 45, 832–839. https://doi.org/10.2135/cropsci2004.0238

Hoffmann, L., Besseau, S., Geoffroy, P., Ritzenthaler, C., Meyer, D., Lapierre, C., Pollet, B., Legrand, M., 2004. Silencing of Hydroxycinnamoyl-Coenzyme A Shikimate/Quinate Hydroxycinnamoyltransferase Affects Phenylpropanoid Biosynthesis. Plant Cell 16, 1446–1465. https://doi.org/10.1105/tpc.020297

Ho-Yue-Kuang, S., Alvarado, C., Antelme, S., Bouchet, B., Cezard, L., Bris, P.L., Legee, F., Maia-Grondard, A., Yoshinaga, A., Saulnier, L., Guillon, F., Sibout, R., Lapierre, C., Chateigner-Boutin, A.L., 2016. Mutation in Brachypodium caffeic acid O-methyltransferase 6 alters stem and grain lignins and improves straw saccharification without deteriorating grain quality. J. Exp. Bot. 67, 227. https://doi.org/10.1093/jxb/erv446

Hu, Y., Li, W.Ch., Xu, Y.Q., Li, G.J., Liao, Y., Fu, F.-L., 2009. Differential expression of candidate genes for lignin biosynthesis under drought stress in maize leaves. J. Appl. Genet. 50, 213–223. https://doi.org/10.1007/BF03195675

Humphreys, J.M., Chapple, C., 2002. Rewriting the lignin roadmap. Curr. Opin. Cell Biol. 5, 224–229. https://doi.org/10.1016/S1369-5266(02)00257-1

Jäger, A., Bader, Th., Hofstetter, K., Eberhardsteiner, J., 2011. The relation between indentation modulus, microfibril angle, and elastic properties of wood cell walls. Compos. Part A Appl. Sci. Manuf. 42, 677–685. https://doi.org/10.1016/j.compositesa.2011.02.007

Jaime, R., Alcántara, J.M., Manzaneda, A.J., Rey, P.J., 2018. Climate change decreases suitable areas for rapeseed cultivation in Europe but provides new opportunities for white mustard as an alternative oilseed for biofuel production. PLOS ONE 13, e0207124. https://doi.org/10.1371/journal.pone.0207124

Jamme, F., Kascakova, S., Villette, S., Allouche, F., Pallu, S., Rouam, V., Réfrégiers, M., 2013. Deep UV autofluorescence microscopy for cell biology and tissue histology. Biol. Cell. 105, 277–288. https://doi.org/10.1111/boc.201200075

Jamme, F., Villette, S., Giuliani, A., Rouam, V., Wien, F., Lagarde, B., Réfrégiers, M., 2010. Synchrotron UV Fluorescence Microscopy Uncovers New Probes in Cells and Tissues. Microsc. Microanal. 16, 507–514. https://doi.org/10.1017/S1431927610093852

Kariuki, L.W., Masinde, P., Githiri, S., Onyango, A.N., 2016. Effect of water stress on growth of three linseed (Linum usitatissimum L.) varieties. Springerplus 5, 759. https://doi.org/10.1186/s40064-016-2348-5

Kelemen, A., Munch, W., Poelman, H., Gakova, Z., Dijkstra, L., Torighelli, B., 2009. The climate change challenge for European regions, in: Regions 2020. European Commission Regional Policy, Brussels.

Kodina L. 2010. Carbon isotope fractionation in various forms of biogenic organic matter: I. Partitioning of carbon isotopes between the main polymers of higher plant biomass. Geochemistry International 48: 1157-1165

Kolodziejski, W., Klinowski, J., 2002. Kinetics of Cross-Polarization in Solid-State NMR: A Guide for Chemists. Chem. Rev. 102, 613–628. https://doi.org/10.1021/cr000060n

Larsson, P.T., Wickholm, K., Iversen, T., 1997. A CP/MAS 13C NMR investigation of molecular ordering in celluloses. Carbohydr. Res. 302, 19–25.

Le Duigou, A., Davies, P., Baley, C., 2011. Environmental Impact Analysis of the Production of Flax Fibres to be Used as Composite Material Reinforcement. J. Biobased Mat. Bioenergy 5, 153–165. https://doi.org/10.1166/jbmb.2011.1116

Le Duigou, A., Davies, P., Baley, C., 2010. Analyse du cycle de vie d'un biocomposite. Mater. et Tech. 98, 143–150. https://doi.org/10.1051/mattech/2010021

Lefeuvre, A., Baley, C., Morvan, C., 2018. Analysis of Flax Fiber Cell-Wall Non-Cellulosic Polysaccharides Under Different Weather Conditions (Marylin Variety). J. Nat. Fibers 15, 539–544. https://doi.org/10.1080/15440478.2017.1349020

Lefeuvre, A., Bourmaud, A., Morvan, C., Baley, C., 2014. Tensile properties of elementary fibres of flax and glass: Analysis of reproducibility and scattering. Mater. Lett. 130, 289–291. https://doi.org/10.1016/j.matlet.2014.05.115

Lion, C., Simon, C., Huss, B., Blervacq, A.-S., Tirot, L., Toybou, D., Spriet, C., Slomianny, C., Guerardel, Y., Hawkins, S., Biot, C., 2017. BLISS: A Bioorthogonal Dual-Labeling Strategy to Unravel Lignification Dynamics in Plants. Cell Chem. Biol. 24, 326–338. https://doi.org/10.1016/j.chembiol.2017.02.009

Macoy, D.M., Kim, W.-Y., Lee, S.Y., Kim, M.G., 2015. Biosynthesis, physiology, and functions of hydroxycinnamic acid amides in plants. Plant Biotechnol. Rep. 9, 269–278. https://doi.org/10.1007/s11816-015-0368-1

Mahfouze, H., Mahfouze, S., El-Enany, M., Ottai, M., 2017. Assessment of Flax Varieties for Drought Tolerance. Annu. Res. Rev. Biol. 21, 1–12. https://doi.org/10.9734/ARRB/2017/38495

Malavasi, U.C., Davis, A.S., Malavasi, M. de M., 2016. Lignin in Woody Plants under Water Stress: A Review. Floresta Ambient. 23, 589–597. https://doi.org/10.1590/2179-8087.143715

Manian, A.P., Cordin, M., Pham, T., 2021. Extraction of cellulose fibers from flax and hemp: a review. Cellulose 28, 8275–8294. https://doi.org/10.1007/s10570-021-04051-x

Mateus NS, Florentino AL, Oliveira JB, Santos EF, Gaziola SA, Rossi ML, Linhares FS, Bendassolli JA, Azevedo RA, Lavres J. 2021. Leaf 13C and 15N composition shedding light on easing drought stress through partial K substitution by Na in eucalyptus species. Sci Rep. 11(1):20158. doi: 10.1038/s41598-021-99710-1.

McMaster, G.S., Wilhelm, W.W., 2003. Phenological responses of wheat and barley to water and temperature: improving simulation models. J. Agric. Sci. 141, 129–147. https://doi.org/10.1017/S0021859603003460

Melelli, A., Arnould, O., Beaugrand, J., Bourmaud, A., 2020. The Middle Lamella of Plant Fibers Used as Composite Reinforcement: Investigation by Atomic Force Microscopy. Molecules 25, 632. https://doi.org/10.3390/molecules25030632

Melelli, A., Durand, S., Arnould, O., Richely, E., Guessasma, S., Jamme, F., Beaugrand, J., Bourmaud, A., 2021. Extensive investigation of the ultrastructure of kink-bands in flax fibres. Ind. Crops Prod. 164, 113368. https://doi.org/10.1016/j.indcrop.2021.113368

Michel, C., Nosch, M.-L. (Eds.), 2010. Textile terminologies in the ancient Near East and Mediterranean from the third to the first millennia BC, Ancient textile series. Oxbow Books, Oxford ; Oakville.

Milthorpe, F.L., 1945. Fibre Development of Flax in Relation to Water Supply and Light Intensity. Ann. Bot. 9, 31–53.

Neutelings, G., 2011. Lignin variability in plant cell walls: Contribution of new models. Plant. Sci. J. 181, 379–386. https://doi.org/10.1016/j.plantsci.2011.06.012

Newman, R.H., 1999. Estimation of the lateral dimensions of cellulose crystallites using 13C NMR signal strengths. Solid State Nucl. Magn. Reson. 15, 21–29. https://doi.org/10.1016/S0926-2040(99)00043-0

Özparpucu, M., Gierlinger, N., Cesarino, I., Burgert, I., Boerjan, W., Rüggeberg, M., 2019. Significant influence of lignin on axial elastic modulus of poplar wood at low microfibril angles under wet conditions. J. Exp. Bot. 70, 4039–4047. https://doi.org/10.1093/jxb/erz180

Özparpucu, M., Rüggeberg, M., Gierlinger, N., Cesarino, I., Vanholme, R., Boerjan, W., Burgert, I., 2017. Unravelling the impact of lignin on cell wall mechanics: a comprehensive study on young poplar trees downregulated for CINNAMYL ALCOHOL DEHYDROGENASE (CAD). Plant J. 91, 480–490. https://doi.org/10.1111/tpj.13584

Petrova, A.A., Kozlova, L.V., Gaifullina, I.Z., Ananchenko, B.A., Martinson, E.A., Mikshina, P.V., Gorshkova, T.A., 2019. AFM analysis reveals polymorphism of purified flax

rhamnogalacturonans I of distinct functional types. Carbohydr. Polym. 216, 238–246. https://doi.org/10.1016/j.carbpol.2019.03.087

Quaglierini, C., 2012. Fibre vegetali da fusto, foglie, frutti e alghe, in: Chimica delle fibre tessili. Zanichelli editore, Bologna, pp. 107–113.

Rasband, W.S., 1997. ImageJ. National Institutes of Health, Bethesda, Maryland, USA.

Réquilé, S., Mazian, B., Grégoire, M., Musio, S., Gautreau, M., Nuez, L., Day, A., Thiébeau, P., Philippe, F., Chabbert, B., Chamussy, A., Shah, D.U., Beaugrand, J., Placet, V., Benezet, J.-C., le Duigou, A., Bar, M., Malhautier, L., De Luycker, E., Amaducci, S., Baley, C., Bergeret, A., Bourmaud, A., Ouagne, P., 2021. Exploring the dew retting feasibility of hemp in very contrasting European environments: Influence on the tensile mechanical properties of fibres and composites. Ind. Crops Prod. 164, 113337. https://doi.org/10.1016/j.indcrop.2021.113337

Richely, E., Bourmaud, A., Placet, V., Guessasma, S., Beaugrand, J., 2021. A critical review of the ultrastructure, mechanics and modelling of flax fibres and their defects. Prog. Mater. Sci. 100851. https://doi.org/10.1016/j.pmatsci.2021.100851

Rihouey, C., Paynel, F., Gorshkova, T., Morvan, C., 2017. Flax fibers: assessing the non-cellulosic polysaccharides and an approach to supramolecular design of the cell wall. Cellulose 24, 1985–2001. https://doi.org/10.1007/s10570-017-1246-5

Rodríguez-Calcerrada, J., Rodrigues, A.M., António, C., Perdiguero, P., Pita, P., Collada, C., Li, M., Gil, L., 2021. Stem metabolism under drought stress – a paradox of increasing respiratory substrates and decreasing respiratory rates. Physiol. Plantarum 172, 391–404. https://doi.org/10.1111/ppl.13145

Šamec, D., Karalija, E., Šola, I., Vujčić Bok, V., Salopek-Sondi, B., 2021. The Role of Polyphenols in Abiotic Stress Response: The Influence of Molecular Structure. Plants 10, 118. https://doi.org/10.3390/plants10010118

Schindelin, J., Arganda-Carreras, I., Frise, E., Kaynig, V., Longair, M., Pietzsch, T., Preibisch, S., Rueden, C., Saalfeld, S., Schmid, B., Tinevez, J.-Y., White, D.J., Hartenstein, V., Eliceiri, K., Tomancak, P., Cardona, A., 2012. Fiji: an open-source platform for biological-image analysis. Nat. Methods. 9, 676–682. https://doi.org/10.1038/nmeth.2019

Schuppler, U., He, P.-H., John, P.C.L., Munns, R., 1998. Effect of Water Stress on Cell Division and Cdc2-Like Cell Cycle Kinase Activity in Wheat Leaves. Plant Physiol. 117, 667–678.

Séverin-Fabiani, T., 2016. Imagerie de photoluminescence synchrotron pour l'étude de matériaux anciens semi-conducteurs (optique/photonique). Université Paris-Sud.

Shah, D.U., Schubel, P.J., Clifford, M.J., 2013. Can flax replace E-glass in structural composites? A small wind turbine blade case study. Compos. B. Eng. 52, 172–181. https://doi.org/10.1016/j.compositesb.2013.04.027

Shankar, A., Agrawal, N., Sharma, M., Pandey, A., Pandey, G.K., 2015. Role of Protein Tyrosine Phosphatases in Plants. Curr. Genomics 16, 224–236. https://doi.org/10.2174/1389202916666150424234300

Sheteiwy, M. S., Abd Elgawad, H., Xiong, Y.-C., Macovei, A., Brestic, M., Skalicky, M., . . . El-Sawah, A. M. (2021). Inoculation with Bacillus amyloliquefaciens and mycorrhiza confers tolerance to drought stress and improve seed yield and quality of soybean plant. 172(4), 2153-2169

Sihel, D.L., 1998. The Biosynthesis of Tryptophan, Tyrosine, and Phenylalanine from Chorismate, in: Singh, B.K. (Ed.), Plant Amino Acids: Biochemistry and Biotechnology. CRC Press, pp. 171–200. https://doi.org/10.1201/9781482270068

Spinoni, J., Naumann, G., Vogt, J.V., Barbosa, P., 2015. The biggest drought events in Europe from 1950 to 2012. J. Hydrol. Reg. Stud. 3, 509–524. https://doi.org/10.1016/j.ejrh.2015.01.001

Stanzl-Tschegg, S., Beikircher, W., Loidl, D., 2009. Comparison of mechanical properties of thermally modified wood at growth ring and cell wall level by means of instrumented indentation tests. Holzforschung 63, 443–448. https://doi.org/10.1515/HF.2009.085

Tedetti, M., Longhitano, R., Garcia, N., Guigue, C., Nicolas, F., Goutx, M., 2012. Fluorescence properties of dissolved organic matter in coastal Mediterranean waters influenced by a municipal sewage

effluent (Bay of Marseilles, France). Environmental Chemistry 9, 439–448. https://doi.org/10.1071/EN12081

van der Werf, H.M.G., Turunen, L., 2008. The environmental impacts of the production of hemp and flax textile yarn. Ind. Crops Prod. 27, 1–10. https://doi.org/10.1016/j.indcrop.2007.05.003

Verhertbruggen, Y., Walker, J.L., Guillon, F., Scheller, H.V., 2017. A comparative study of sample preparation for staining and immunodetection of plant cell walls by light microscopy. Front. Plant Sci. 8, 1505. https://doi.org/10.3389/fpls.2017.01505

Vidot, K., Devaux, M.-F., Alvarado, C., Guyot, S., Jamme, F., Gaillard, C., Siret, R., Lahaye, M., 2019. Phenolic distribution in apple epidermal and outer cortex tissue by multispectral deep-UV autofluorescence cryo-imaging. Plant Science 283, 51–59. https://doi.org/10.1016/j.plantsci.2019.02.003

Vogeslang-Eastwood, G., 2000. Textiles, in: Nicholson, P.T., Shaw, I. (Eds.), Ancient Egyptian Materials and Technology. Cambridge University Press, pp. 268–297.

Waldron, K.W., Parr, A.J., Ng, A., Ralph, J., 1996. Cell wall esterified phenolic dimers: identification and quantification by reverse phase high performance liquid chromatography and diode array detection. Phytochem. Anal. 7, 305–312.

Wilhite, D.A., Glantz, M.H., 1985. Understanding: the Drought Phenomenon: The Role of Definitions. Water Int. 10, 111–120. https://doi.org/10.1080/02508068508686328

Zhao, Y., 2010. Auxin biosynthesis and its role in plant development. Annu. Rev. Plant. Biol. 61, 49–64. https://doi.org/10.1146/annurev-arplant-042809-112308

APPENDIX

Figure A1. Overview of the sample route analysis for Synchrotron DISCO beamline exploration.

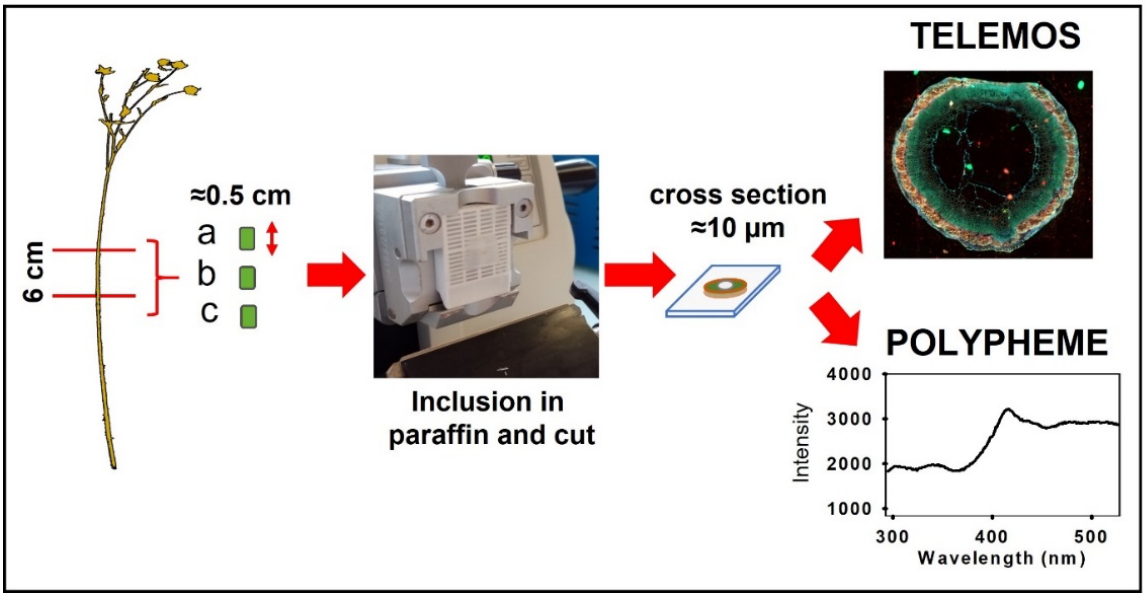

The suitability of the three filters has been discussed in terms of their appropriateness to capture the most important differences in the biochemical composition of flax stems under stress.

The acquired images must be corrected to quantitatively calculate the fluorescence intensity. **Equ. A.1** is used to normalize the grey level to eliminate the variations linked to the CCD camera for each filter and acquisition time, as well as the heterogeneity of the intensity linked with the laser beam:

$$I_c = \frac{I_r - D_{(f,t)}}{W_{(z)} - D_{(w)}} \qquad \text{(A.1)}$$

where I_c is the grey level in the corrected image, I_r is the level in the raw image acquired, $D_{(f,t)}$ is the "dark" level of the camera acquired depending on the filter used and the acquisition time, $W_{(z)}$ is the "white" level of the beam without filters depending on the Z stack position and objective used and $D_{(w)}$ is the "dark" level acquired to record the noise of the instrument without any filter (Vidot et al., 2019). To perform the 'white' level, a small window of luminescent reference compound (Nd-YAG crystal) using only the dichroic mirror without any filter was used as a reference.

With TELEMOS, the three stems of the two batches, each with three cross-sections, were analysed in a total of 18 cross-sections, 9 from drought plants and 9 from control plants. The images acquired were ultimately processed using ImageJ/Fiji software (Rasband, 1997; Schindelin et al., 2012). Segment and area tools were used to select ROI and calculate the intensity of each filter in regions of the image where the beam intensity is focused, i.e. the centre of the image (**Figure A.2**). For further information on the method, see (Beaugrand et al., 2022).

A range of display values for each channel and each objective was fixed (10x objective: red 0–1500; green 0–2500; blue 0–2500; and 40x objective: red 0–1500; green 0–4000; blue 0–4000) to obtain similar colour intensity in images acquired with the two different objectives.

Figure A.2 TELEMOS images acquired and processed. Illustration given for the control sample. The images are 16-bit (65536 grey levels) composite images resulting from the three filters. The region of interest (ROI) where fluorescence intensity was calculated is highlighted in red. Images acquired with a 40x objective.

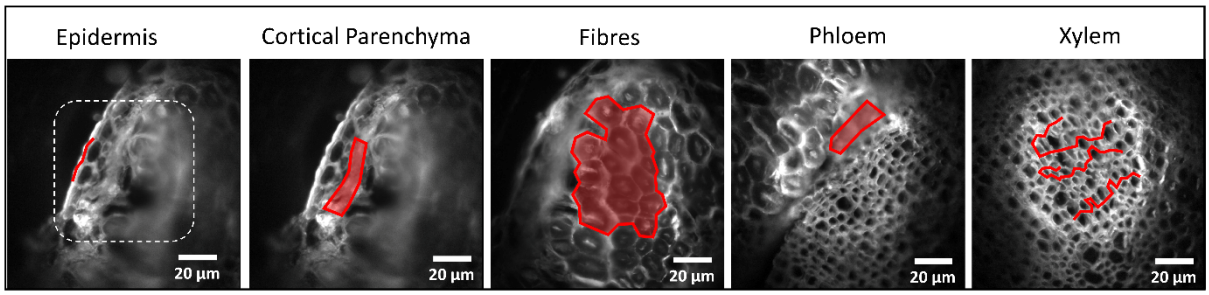

Figure A.3 Fluorescence spectra extracted from the cross section of the control and drought stem sample. Illustration of the epidermal cell type and paraffin, which does not fluoresce (background).